Master's Thesis
석사 학위논문

Age of Information Analysis in Hyperledger Fabric Blockchain-enabled Wireless Monitoring Networks.

Minsu Kim (김 민 수 金 珉 秀)

Department of
Information & Communication Engineering

DGIST

2020

Master's Thesis
석사 학위논문

Age of Information Analysis in Hyperledger Fabric Blockchain-enabled Wireless Monitoring Networks.

Minsu Kim (김 민 수 金 珉 秀)

Department of
Information & Communication Engineering

DGIST

2020

Age of Information Analysis in Hyperledger Fabric Blockchain-enabled Wireless Monitoring Networks.

Advisor: Professor Jemin Lee
Co-advisor: Professor Jeonghun Park

by

Minsu Kim
Department of Information & Communication Engineering

DGIST

A thesis submitted to the faculty of DGIST in partial fulfillment of the requirements for the degree of Master of Science in the Department of Information & Communication Engineering. The study was conducted in accordance with Code of Research Ethics[1]

25. 11. 2020

Approved by

Professor Jemin Lee (Advisor) (signature)

Professor Jeonghun Park (Co-Advisor) (signature)

[1] Declaration of Ethical Conduct in Research: I, as a graduate student of DGIST, hereby declare that I have not committed any acts that may damage the credibility of my research. These include, but are not limited to: falsification, thesis written by some-one else, distortion of research findings or plagiarism. I affirm that my thesis contains honest conclusions based on my own careful research under the guidance of my thesis advisor.

Age of Information Analysis in Hyperledger Fabric Blockchain-enabled Wireless Monitoring Networks.

Minsu Kim

Accepted in partial fulfillment of the requirements for the degree of Master of Science.

25. 11. 2020

Head of Committee Prof. Jemin Lee (signature)

Committee Member Prof. Jeonghun Park (signature)

Committee Member Prof. Kyungjoon Park (signature)

ABSTRACT

Age of Information (AoI) is a recently proposed metric for quantifying data freshness in real-time status monitoring systems where timeliness is of importance. In this paper, we explore the data freshness in Hyperledger Fabric Blockchain-enabled monitoring network (HeMN) by leveraging the AoI metric. In HeMN, status updates from sources are transmitted through an uplink and recorded in the Hyperledger Fabric (HLF) network. To investigate the characteristics of the AoI in HeMN, we formulate the distribution of peak age of information (PAoI) and the average AoI. Furthermore, we derive a closed-form of the AoI violation probability, considering the transmission latency and the consensus latency for a stochastic guarantee of data freshness. We validate the analytic results by implementing a HLF network. We also investigate the effects of the parameters in HeMN, i.e., a target successful transmission probability (STP), block size, and timeout, on the average AoI, PAoI violation probability, and AoI violation probability and show a trade-off relationship exists between them. Then, we conclude by providing the design insights into keeping data fresh in HeMN.

Keywords: Age of information, blockchain, Hyperledger Fabric, latency, stochastic geometry

List of Contents

List of Tables

List of Figures

I. INTRODUCTION

1.1 Backgrounds

Recent advances in wireless communications and IoT devices have led to an increase in applications that leverage real-time data. Especially, real-time status monitoring systems have been deployed worldwide for time-critical applications such as traffic management in vehicle systems, pollution detection, and autonomous factories. These systems usually consist of a source and a destination. Specifically, the source generates a status update (or a packet) with observed information and transmits it to the destination where status updates (or packets) are received and recorded. In these systems, decisions are made based on the observed information from the source. For instance, raising an alarm about a high level of pollution or temperature can be one of the decisions made from the observed information. In such cases, outdated data may lead to incorrect decisions. In this regard, therefore, it is of importance for real-time status monitoring systems to provide fresh data, in order to prevent undesirable outputs. To quantify the degree of data freshness, AoI has been proposed in [1]. It is defined as the elapsed time from the generation of the latest received status update.

1.2 Related Work

The initial work of the AoI focuses on the characteristics of the AoI for various queueing systems [1–4]. In [1], the optimal sampling rate to minimize the average AoI for M/M/1, M/D/1, and D/M/1 is obtained. The optimal sampling rate to minimize average AoI in the multi source cases for M/M/1 is considered in [2]. Besides, peak age of information (PAoI) is introduced for M/M/1 queueing systems with one or two queueing length [3]. Note that PAoI refers to the AoI just before an update instant. In [4], the stationary distribution of the AoI for general first-come-first-serve (FCFS) queueing systems is analyzed in terms of the system delay and PAoI.

To characterize the probability of violating a certain threshold, the AoI violation probability is also analyzed in [5–8]. The upper bound of the tail of the AoI distribution for D/G/1 queueing systems is formulated to find an optimal sampling rate that minimizes the AoI violation probability in [5]. Similarly, the outage probability of PAoI is characterized for the same queueing systems aforementioned [6]. The AoI violation probability is analyzed in [7] for GI/GI/1/1 and GI/GI/1/2* queues of non-preemptive scheduling systems. In [8], the delay and the PAoI violation probability are analyzed under FCFS queue in the finite block-length regime, which encompasses automatic repetition request (ARQ) and hybrid automatic repetition request (HARQ).

The AoI has also been analyzed for real-time IoT applications in order to capture the timeliness of monitoring data [9–11]. In [9], the optimal sampling policy is obtained to minimize the weighted sum-AoI in energy harvesting enabled IoT networks. In [10], the average AoI penalty function of an energy harvesting IoT system is obtained and the status update frequency is optimized to minimize the average AoI penalty. An AoI-energy trade-off is studied for IoT monitoring systems and the average AoI is minimized by optimizing the transmission power of an IoT device in [11]. However, all of the previous papers did not consider the case when information is stored in a blockchain, which cannot guarantee data integrity.

Recently, a blockchain has been regarded as a promising decentralized data management platform for IoT devices aiming to eliminate the need of a central authority [12]. The integration of blockchain platforms and IoT devices are studied in [13–16]. A blockchain integrated IoT platform is presented for real-time monitoring with the aim of providing data integrity [13]. In [14], the communication cost of periodic updates is analyzed in Ethereum blockchain for lightweight IoT devices, which only store the head of blocks. In [15], the effects of network configurations (i.e., the number of hops and nodes) on the end-to-end delay are studied in blockchain platforms for IoT applications. For the blockchain-enabled wireless IoT network, the optimal deployment of the nodes for maximizing transaction throughput is investigated in [16].

However, data freshness in blockchain platforms is not analyzed in the previous papers [13–16], which fails to show the timeliness of stored data. In the case of monitoring networks, blockchain technology has lately drawn attention because the data integrity issue in monitoring networks can be resolved, although the data freshness issue is left unsettled. For instance, a blockchain may be selected as the underlying system of an alarm system (e.g., pollution or fire detection) in order to ensure data integrity. However, this system requires not only the integrity of monitored data, but also the timeliness of it. If any of the two properties are not satisfied, the system may result in a wrong decision [17]. Therefore, in this paper, we analyze the data freshness in a blockchain platform, where the integrity of recorded data is guaranteed.

A blockchain utilizes a hash function to form a transaction chain, to provide data integrity in a distributed manner. Therefore, it requires an additional latency spent to process transactions, while status updates are finished promptly at destinations in the previous AoI papers [1–11]. Only in [18], the average AoI is investigated for a public blockchain and the IOTA platform, which utilizes a directed acyclic graph. However, although both the transmission time and the latency for the consensus process are considered, it is difficult to show how much the timeliness of the status update is guaranteed because this paper only explores the average AoI. Moreover, the AoI in a permissioned blockchain is not considered in [18]. Unlike a public blockchain, users are all identified in a permissioned blockchain. This strict membership rule makes computationally intensive consensus protocols (e.g.,proof-of-work (PoW)) unnecessary, hence, a permissioned blockchain platform may be more suitable for managing IoT devices. In this regard, we consider the HLF platform, which is one of the most utilized permissioned blockchain platform. In HLF, the latest monitored information is stored in a distributed ledger with its history, which can provide data integrity.

1.3 Contributions

In this paper, we investigate the data freshness in HeMN, where sources observe physical phenomena and update their status in the HLF network, which is connected to BSs. Sources and BSs are distributed randomly in the network, and each source transmits a packet to its nearest BS. To measure the freshness of data in HeMN, the AoI is utilized. The distribution of PAoI and the expression for the average AoI for HeMN are obtained. We then analyze the AoI violation probability, which shows the probability that the AoI exceeds a given target AoI. Furthermore, we analyze the effects of communication and HLF parameters on the average AoI, PAoI violation probability, and AoI violation probability. Our main contributions can be summarized as follows:

- We present the characteristics of the AoI for HeMN including the average AoI, PAoI violation probability, and AoI violation probability in a closed-form by considering the consensus latency in a HLF network as well as the transmission latency.
- We explore the effects of the influential factors on HeMN, i.e., the communication parameter: target STP and HLF parameters: block size and timeout. We also show that a trade-off relationship exists between the parameters of HeMN and the average AoI, PAoI violation probability, and AoI violation probability. Then, we provide some design insights into keeping data fresh in HeMN.

- We validate the analytical results by implementing the HLF platform v1.3. The results show that our analytical results can precisely reflect the AoI in HeMN.

The remainder of this paper is organized as follows: Section II introduces the overall transaction flow in HLF and the parameters of HLF. Section III describes the HLF blockchain-enabled monitoring network and models the consensus latency. Section IV derives the distribution of PAoI, average AoI, and AoI violation probability in HeMN. Section V provides the validation of the analytical results and effects of the parameters of HeMN on the AoI violation probability. Finally, the conclusions are given in Section VI.

II. Hyperledger Fabric

In this section, we provide the overall structure of HLF and the components of the consensus process for a status update. We also introduce the HLF parameters which affect the performance of HeMN.

2.1 HLF Transaction Flow

HLF is a permissioned blockchain platform, where all changes made by transactions are committed to the distributed ledger. In HLF, peer nodes (or peers) hold their own copied distributed ledgers. The ledger is a key-value database, which consists of two parts: a blockchain and a world state. In the blockchain, the immutable records of status changes are stored. The world state is also a database, where the current value of status for the corresponding key with its current version number is stored. Hence, all data in the ledger is identified by each own key and version number. A transaction is executed against the specified function to update the stored data in the ledger with each corresponding key. In this paper, we assume transactions are to update the status of the sources. In HLF, participants are all identified. Therefore, the costly consensus method in public blockchains, which is known as mining, is not necessary for HLF. Instead, the consensus process in HLF is composed of three phases: endorsing phase, ordering phase, and validation phase as described below. More detailed explanations on each phase are available in [19] [20].

2.1.1 Endorsing Phase

All transactions for status updates enter the endorsing phase first. The endorsing phase is to receive endorsements from the peers, which are entitled to simulate transactions against their own copied ledgers. The peers make sure that they have the exactly identical simulation results, which are referred to as the endorsements. The endorsement includes the updated status and version number of the ledger in the peer. Then, the transaction with the endorsements is transmitted to the ordering node. Note that, although the transaction simulation results are already prepared, the status is not updated in this phase.

2.1.2 Ordering Phase

The ordering phase is not only to arrange transactions in chronological order but also to generate new blocks with the ordered transactions. The ordering nodes continuously include transactions into a new block until it reaches the pre-defined maximum block size. Besides, to avoid high latency, a timer is prepared with the pre-defined timeout value. If the timer expires, the nodes instantly export the new block, regardless of the current number of transactions in the block. The newly generated block is then delivered to the peers by the ordering nodes.

2.1.3 Validation Phase

The validation phase is to validate the delivered block to the peers and to update the ledger. This phase consists of two sequential steps: verification and update. The peers investigate if each transaction in the block is properly endorsed from the endorsement phase. Then, the peers check whether the version numbers in the endorsements are identical to the ones currently stored in their copied ledgers. This verification is also called the MVCC verification. Note that the version number increases each time the corresponding status is updated. Hence, if the two version numbers are different, this signifies that the status already has been updated by the previous transaction before the current one completes the consensus process. In case the version numbers are different, the transaction is marked as invalid and becomes ineffective. Lastly, the peers update the world state and the blockchain in the ledger.

2.2 HLF Parameters

The HLF parameters refer to HLF platform configurations, which are the block size and the block-generation timeout. As introduced in the ordering phase section, those parameters control how long a transactions will wait in the ordering phase, which affects the consensus latency.

2.2.1 Block Size, $\hat{B}$

The block size limits the maximum number of transactions in a block. A newly arrived transaction needs to wait in the ordering phase until the number of transactions in the block reaches the block size. Therefore, larger block sizes make transactions wait longer as more time is required to fill up the block.

2.2.2 Timeout, $\hat{T}$

The timeout is another way to limit the waiting time of a transaction in the ordering phase. The transaction can wait up to timeout value for other transactions in the ordering phase. The new block can move to the next phase even if the block is not completely full to avoid long latency. As can be expected, transactions generally need to wait longer as the timeout increases.

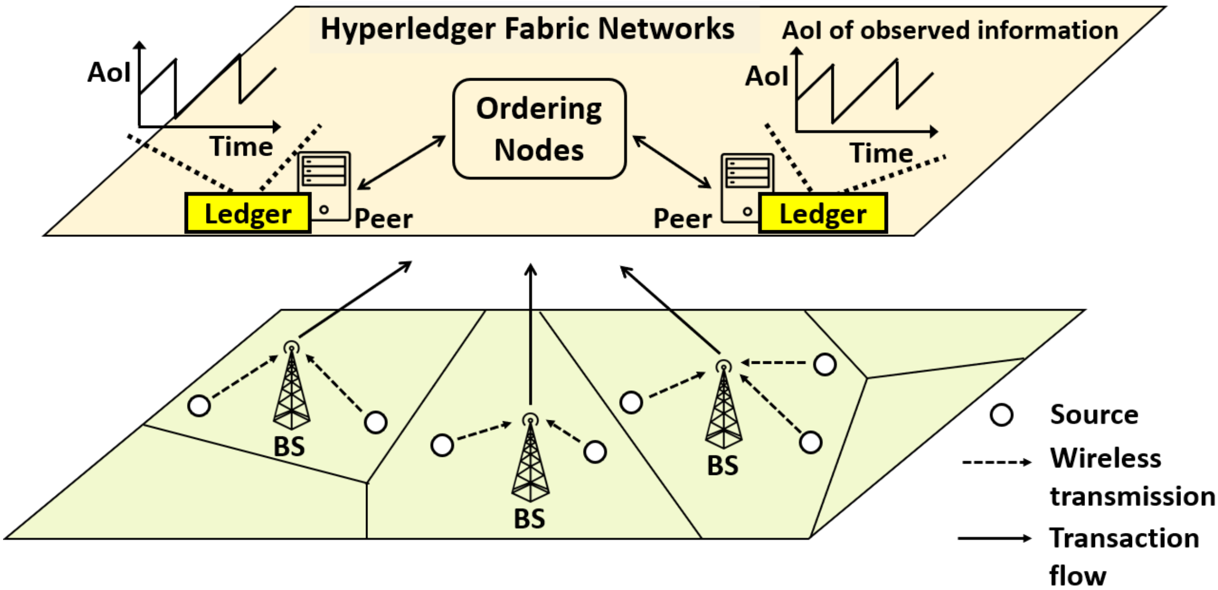

Figure 2.1: The HeMN composed of the sources, the BSs, and HLF network.

III. HLF Blockchain-Enabled Monitoring Network

3.0.1 System Model

We consider the HeMN composed of sources, BSs, and HLF network, where sources monitor physical phenomena (e.g., temperature, pollution level) and update the corresponding status stored in HLF as shown in Fig. 2.1. We assume the distribution of the sources follows a homogeneous Poisson Point Process (HPPP) Φ_s with spatial density λ_s. The source transmits a packet through a wireless uplink channel to the nearest BS [21] [22]. We assume that all the sources use the same transmission power P. The distribution of BSs also follows a HPPP Φ_m with spatial density λ. Each channel is allocated to one source only in the cell of a BS to avoid the interference between the sources in the same cell.

We assume BSs are connected to HLF network, where the status information of sources are stored with their own key values. As shown in Fig. 2.1, a source monitors a physical phenomenon and generates a packet with newly observed information. The packet is delivered to HLF via a BS in a form of transaction. Successfully received transactions can update their status information through the consensus process, which is described in Sec. 2.1.

We define the consensus latency as the total time, required for the commitment of a transaction, which is the summation of the latencies in each phase. Then, the total latency of the kth packet can be defined as

$$T_{\text{tot},k} = X_k + T_{\text{tra}}, \tag{3.1}$$

where X_k is the consensus latency of the kth packet and T_{tra} denotes the transmission latency required for transmitting a packet from a source to its associated BS. The consensus latency $\{X_k, k \geq 1\}$ is assumed to be independent and identically distributed (i.i.d.).

3.0.2 Consensus Latency Modeling

In this subsection, we model the consensus latency in HeMN. From empirical results of a constructed HLF platform, it is shown that the Gamma distribution is reasonable for modeling the consensus latency in the HLF platform [SlMKJl:20]. Then, the consensus latency for the kth packet X_k can be modeled as a Gamma random variable, of which probability density function (PDF) is given by [23]

$$f_{X_k}(x) = \frac{\beta^\alpha}{\Gamma(\alpha)} x^{\alpha-1} e^{-\beta x}, \tag{3.2}$$

where α and β are the shape and the rate parameters, respectively, and $\Gamma(\cdot)$ is a Gamma function. To determine the values of α and β for the consensus latency, we can use the maximum likelihood estimation [23]. Specifically, α and β can be given by

$$\alpha = \frac{1}{4A}\left(1 + \sqrt{1 + \frac{4A}{3}}\right)$$
$$\beta = \frac{\alpha}{\bar{X}}, \tag{3.3}$$

where $\bar{X}$ is the mean of consensus latencies and A is given by

$$A = \log(\bar{X}) - \sum_{i=1}^{N} \log(X_i)/N \tag{3.4}$$

for the sample consensus latency X_i and N number of samples. We use the Kolmogorov-Smirnov (KS) test [24], [25] to investigate the accuracy of the modeling, of which results are provided in Sec. 5.0.1. Note that this modeling of consensus latency is applicable to general HLF with version 1.0 or higher [1].

3.0.3 Analysis of Transmission Latency

In this subsection, we analyze the transmission latency T_{tra} of HeMN [26]. The signal to interference plus noise ratio (SINR) received by a BS at $\mathbf{y}_{\text{o}}$ from a source located at $\mathbf{x}_{\text{o}}$ under Rayleigh fading channel is given by

$$\text{SINR} = \frac{P h_{\mathbf{x}_{\text{o}},\mathbf{y}_{\text{o}}} L_{\mathbf{x}_{\text{o}},\mathbf{y}_{\text{o}}}^{-n}}{I + N_0 W}, \tag{3.5}$$

where $h_{\mathbf{x}_{\text{o}},\mathbf{y}_{\text{o}}}$ is the fading channel gain, i.e., $h_{\mathbf{x}_{\text{o}},\mathbf{y}_{\text{o}}} \sim \exp(1)$, N_0 is the noise power, W is the channel bandwidth, $L_{\mathbf{x}_{\text{o}},\mathbf{y}_{\text{o}}}$ is the distance between the source at $\mathbf{x}_{\text{o}}$ and the associated BS at $\mathbf{y}_{\text{o}}$, and n is the pathloss exponent. In (3.5), I is the interference from other sources that use the same uplink frequency band, given by

$$I = P \sum_{\mathbf{x} \in \Psi_u \setminus \mathbf{x}_{\text{o}}} h_{\mathbf{x},\mathbf{y}_{\text{o}}} L_{\mathbf{x},\mathbf{y}_{\text{o}}}^{-n}, \tag{3.6}$$

[1] HLF with version 1.0 or higher includes the MVCC verification

where Ψ_u denotes the set of locations of the sources which use the same frequency band with the source at $\mathbf{x}_\mathrm{o}$. Then, the data rate R is given by

$$R = W \log_2(1 + \mathrm{SINR}). \tag{3.7}$$

The STP, denoted by p_c, is defined as the probability that data rate is equal or larger than the target rate $\bar{R}$, which is given by

$$p_c = \mathbb{P}\left[R \geq \bar{R}\right]. \tag{3.8}$$

To guarantee a certain level of STP, we can set the target rate $\bar{R}$ as [27]

$$p_c = \mathbb{P}\left[C \geq \bar{R}\right] \geq \zeta, \tag{3.9}$$

where ζ is the target STP. Using (3.9), we can then define the transmission latency as

$$T_{\mathrm{tra}} = \frac{D}{\bar{R}}, \tag{3.10}$$

where D [bits] is the packet size. In (3.10), $\bar{R}$ can be obtained by

$$\bar{R} = \int_0^\infty \bar{R}(r) f_L(r) dr, \tag{3.11}$$

where $f_L(r)$ is the PDF of the distance L between the source and its nearest BS, which follows a Rayleigh distribution as [28].

$$f_L(r) = 2\lambda\pi r \exp(-\lambda\pi r^2). \tag{3.12}$$

In (3.11), $\bar{R}(r)$ is the target rate when the distance between the source and its nearest BS is r, i.e., $L_{\mathbf{x}_o,\mathbf{y}_o} = r$. To obtain $\bar{R}(r)$, we use STP in (3.9), which can be given by

$$p_c = \mathbb{P}\left[\mathrm{SINR} \geq 2^{\frac{\bar{R}(r)}{W}} - 1\right] \geq \zeta. \tag{3.13}$$

From the definition of SINR in (3.5), p_c can be given by

$$p_c = \exp\left(-\frac{r^n}{P} N_0 W \theta\right) \mathbb{E}_I\left[\exp\left(-\frac{r^n}{P} I\theta\right)\right], \tag{3.14}$$

where $\theta = 2^{\bar{R}(r)/W} - 1$ by using the cumulative distribution function (CDF) of the exponential random variable $h_{\mathbf{x}_o,\mathbf{y}_o}$.

Note that the dependence among the locations of interfering sources exists, so their distribution does not follow HPPP. Nevertheless, it is shown that this dependency can be weak [29], so we assume the distribution of the interfering sources follows the HPPP with spatial density λ. A channel is allocated to one source only in the cell of a BS, so the density of uplink interfering sources is λ. According to [30, eq.3.21], Laplace transform of I can be given by

$$\mathcal{L}_I(s) = \exp\left\{-\lambda\pi s^{2/n}\frac{2\pi}{n\sin(2\pi/n)}\right\}. \tag{3.15}$$

From (3.15), p_c in (3.14) can be presented as

$$p_c = \exp\left(-\frac{r^n}{P}N_0W\theta\right)\exp\left\{-\lambda\pi^2\frac{2r^2\theta^{2/n}}{n\sin\left(2\pi/n\right)}\right\}. \tag{3.16}$$

Since it is difficult to present $\bar{R}(r)$ in a closed form from (3.13) and (3.16) with the general pathloss exponent, we set $n=4$ for tractability. We can then present $\bar{R}(r)$ as

$$\begin{aligned}\bar{R}(r) &= W\log_2\left[1+\left\{\frac{P(-\pi^2\lambda+\sqrt{\pi^4\lambda^2-16N_0W\log\zeta})}{4N_0Wr^2}\right\}^2\right]\\ &= W\log_2\left\{1+\left(\frac{m}{r^2}\right)^2\right\},\end{aligned} \tag{3.17}$$

where m is

$$m = \frac{P(-\pi^2\lambda+\sqrt{\pi^4\lambda^2-16N_0W\log\zeta})}{4N_0W}. \tag{3.18}$$

By substituting (3.17) with (3.11) and replacing r^2 with t, $\bar{R}$ is given by

$$\begin{aligned}\bar{R} &= \lambda\pi W\int_0^\infty \log_2\left\{1+\left(\frac{m}{t}\right)^2\right\}\exp(-\lambda\pi t)dt\\ &= \frac{\lambda\pi W}{\log 2}\int_0^\infty \left[\log\left\{t^2+m^2\right\}-\log(t^2)\right]\exp(-\lambda\pi t)dt.\end{aligned} \tag{3.19}$$

Using the results in [31, eq. 4.331, eq. 4.338], $\bar{R}$ in (3.19) can be given by

$$\bar{R} = \frac{W}{\log 2}\left\{\log m - \mathrm{Ci}(m\lambda\pi)\cos(m\lambda\pi) - \mathrm{Si}(m\lambda\pi)\sin(m\lambda\pi) + C + \log(\lambda\pi)\right\}, \tag{3.20}$$

where $\mathrm{Ci}(x)$ and $\mathrm{Si}(x)$ are cosine integral and sine integral, respectively and C is an Euler constant. Using (3.20) and (3.10), the transmission latency T_{tra} is given by

$$T_{\mathrm{tra}} = \frac{D\log 2}{W}\left[\log m - \mathrm{Ci}(m\lambda\pi)\cos(m\lambda\pi) - \mathrm{Si}(m\lambda\pi)\sin(m\lambda\pi) + C + \log(\lambda\pi)\right]^{-1}. \tag{3.21}$$

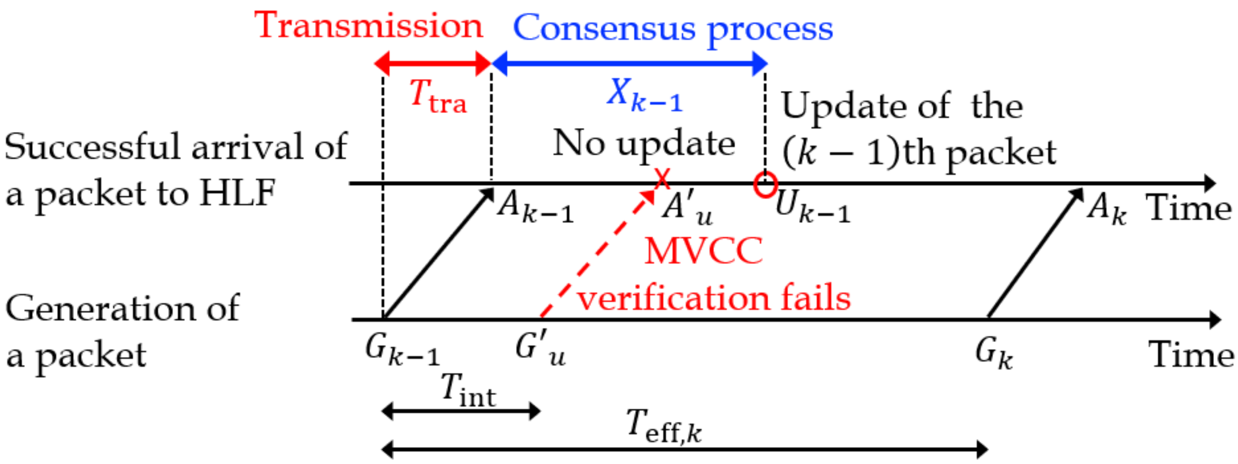

Figure 3.1: MVCC verification failure of the packet generated at G'_u.

IV. AoI Analysis of HeMN

In this section, we analyze the AoI violation probability for HeMN. As a metric for measuring the data freshness, the AoI is defined as the elapsed time since the generation of the last received packet [1]. We focus on a specific status of interest, which is stored with a certain key value in the ledger. As depicted in Fig. 3.1, in HeMN, not every generated packet can make a valid update because of the MVCC verification. If the status is updated before the current packet completes its consensus process, this packet is then marked as invalid and becomes ineffective. We call the packets that make valid updates as *effective packets*. For the kth effective packet, we denote G_k as the generation instant at the source, A_k as the arrival instant at the BS, and U_k as the update instant for the ledger. In addition, G'_u and A'_u are for the generation instant and the arrival instant of the uth invalid packet, respectively. We also define the inter-generation time of effective packets $T_{\text{eff},k}$ as $T_{\text{eff},k} = G_k - G_{k-1}$.

As shown in Fig. 3.1, the kth packet can be effective only if its arrival instant A_k is after U_{k-1}, which is the update instant of the previous $(k-1)$th effective packet. Considering the transmission latency T_{tra} and the total latency of the $(k-1)$th effective packet $T_{\text{tot},k-1}$, any generated packet after X_{k-1} can be an effective packet. It is assumed that the source generates a packet with exponentially distributed inter-generation time with rate ρ_{s} [32] [33]. The inter-generation time of the two consecutive packets that successfully arrive at the BS from the source is denoted as T_{int} and we consider exponentially distributed T_{int} with rate $\rho = \rho_{\text{s}} p_c$. Due to the memoryless property of T_{int}, $T_{\text{eff},k}$ can also be defined as

$$T_{\text{eff},k} = X_{k-1} + T_{\text{int}}. \tag{4.1}$$

The PAoI is the AoI just before the update instant. As shown in Fig. 4.1, for the kth effective packet, PAoI_k is given by

$$\text{PAoI}_k = T_{\text{eff},k} + T_{\text{tot},k}. \tag{4.2}$$

From (4.1) and (4.2), we derive the average AoI $\bar{\Delta}$ for HeMN in the following lemma.

Lemma 1. In HeMN, the average AoI $\bar{\Delta}$ is given by

$$\bar{\Delta} = \frac{\rho\beta}{2(\alpha\rho+\beta)} \left(\frac{2}{\rho^2} + \frac{2\alpha}{\rho\beta} + \frac{\alpha^2+\alpha}{\beta^2} \right) + \frac{\alpha}{\beta} + T_{\text{tra}}, \tag{4.3}$$

where α and β are defined in (3.3), $\rho = \rho_s \rho_c$ and T_{tra} is in (3.21)

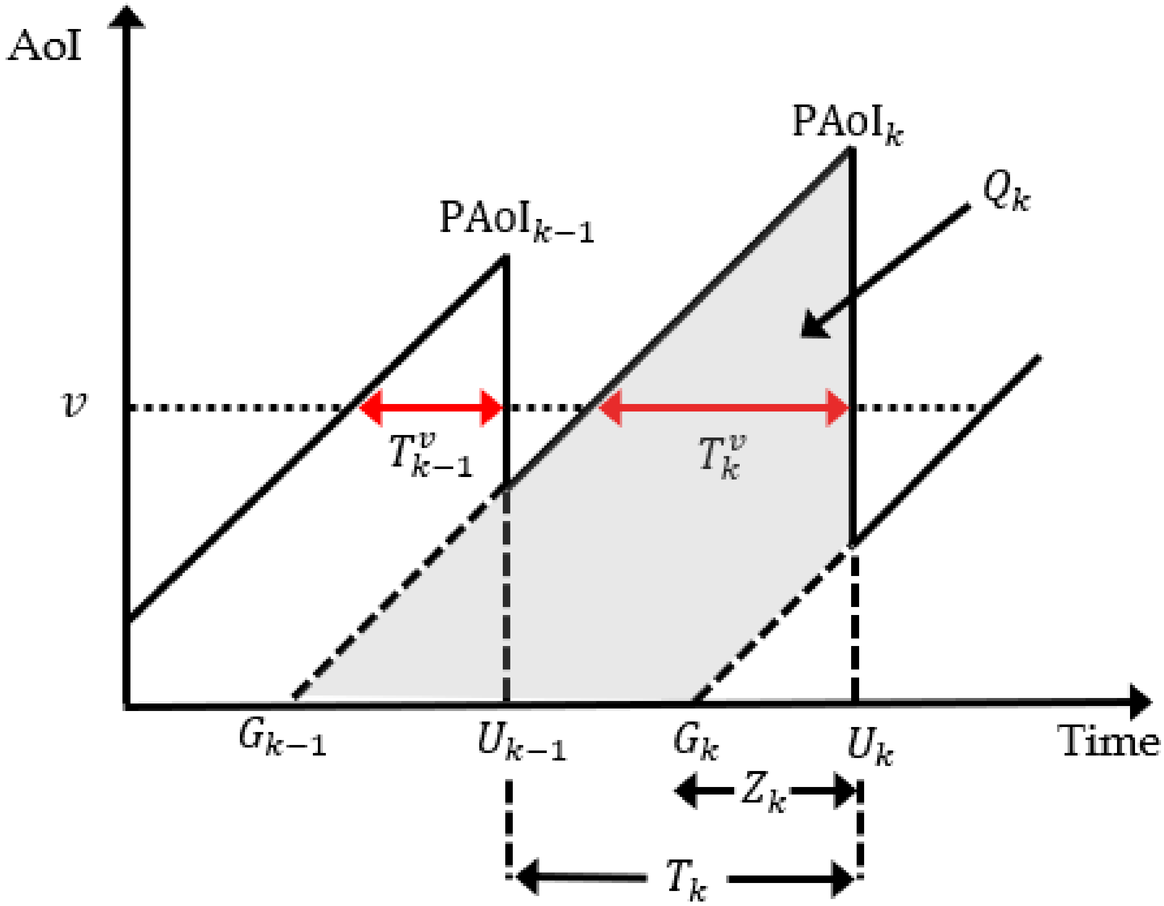

Figure 4.1: A sample path of the AoI where G_k and U_k are the generation instant and the update instant of the kth effective packet.

Proof. We denote the AoI at time t as $\Delta(t) = t - G(t)$, where $G(t)$ represents the time instant for the generation of the latest update, which can be given by $G(t) = \max\{G_k \mid U_k \leq t\}$. Let Q_k represent the area of the trapezoid between U_k and U_{k-1} as shown in Fig. 4.1. From [34], $\bar{\Delta}$ can be given by

$$\begin{aligned}
\bar{\Delta} &= \lim_{T\to\infty} \frac{1}{T}\int_0^T \Delta(t)dt = \lim_{T\to\infty}\frac{1}{T}\sum_{k=1}^{N(T)} Q_k \\
&= \lim_{T\to\infty}\frac{N(T)}{T}\frac{1}{N(T)}\sum_{k=1}^{N(T)} Q_k \\
&\overset{(a)}{=} \lim_{T\to\infty}\frac{\sum_{k=1}^{N(T)} Q_k/N(T)}{\sum_{k=1}^{N(T)}(U_k - U_{k-1})/N(T)} \\
&\overset{(b)}{=} \frac{\mathbb{E}[Q_k]}{\mathbb{E}[T_k]},
\end{aligned} \tag{4.4}$$

where $N(T)$ is the number of updates until time T, defined as $N(T) = \max\{k \mid U_k \leq T\}$. In (4.4), (a) is from the fact that T can be presented in an infinite summation of the update intervals $U_k - U_{k-1}$ as T goes to infinity, and (b) is from the ergodicity of the sample path. In (4.4), Q_k can be calculated by $Q_k = \frac{1}{2}(\mathrm{PAoI}_k^2 - T_{\mathrm{tot},k}^2)$. Therefore, $\mathbb{E}[Q_k]$ can be obtained by

$$\begin{aligned}
\mathbb{E}[Q_k] &= \frac{1}{2}\mathbb{E}[\mathrm{PAoI}_k^2 - T_{\mathrm{tot},k}^2] \\
&= \frac{1}{2}\mathbb{E}[T_{\mathrm{eff},k}^2 + 2T_{\mathrm{eff},k}T_{\mathrm{tot},k}],
\end{aligned} \tag{4.5}$$

where the last equality is from the definition of PAoI_k in (4.2). Using the definitions of $T_{\mathrm{eff},k}$ in (4.1), $\mathbb{E}[Q_k]$ can be given as

$$\mathbb{E}[Q_k] = \frac{1}{2}\mathbb{E}[(T_{\mathrm{int}} + X_{k-1})^2] + \mathbb{E}[(T_{\mathrm{int}} + X_{k-1})(X_k + T_{\mathrm{tra}})]. \tag{4.6}$$

We assume independence between T_{int} and $\{X_k, \forall k \geq 1\}$ in HeMN, then (4.6) can be given by

$$\mathbb{E}[Q_k] = \frac{2}{\rho^2} + \frac{2\alpha}{\rho\beta} + \frac{\alpha^2+\alpha}{\beta^2} + \left(\frac{1}{\rho} + \frac{\alpha}{\beta}\right)\left(\frac{\alpha}{\beta} + T_{\mathrm{tra}}\right). \tag{4.7}$$

In (4.4), as shown in Fig. 4.1, T_k represents the interval of the update instants between U_{k-1} and U_k, which can be given by

$$T_k = T_{\mathrm{eff},k} + T_{\mathrm{tot},k} - T_{\mathrm{tot},k-1} = X_k + T_{\mathrm{int}}. \tag{4.8}$$

Hence, the expectation of T_k is $\mathbb{E}[T_k] = \dfrac{1}{\rho} + \dfrac{\alpha}{\beta}$. The average AoI $\bar{\Delta}$ can be derived by substituting (4.7) and (4.8) into (4.4).

□

From Lemma 1, we can obtain $\bar{\Delta}$ in HeMN, which shows the overall freshness of status information stored in ledgers. To see whether a certain level of freshness is guaranteed in HeMN, we can evaluate the AoI violation probability based on the sample path analysis introduced in [7]. We define $P_v = \mathbb{P}[\mathrm{AoI} \geq v]$,

$$P_v = \frac{\rho\beta^{2\alpha+1}}{(\beta+\rho\alpha)\,\Gamma(\alpha)^2}\sum_{n=0}^{\infty}\frac{(\rho-\beta)^n}{n!(\alpha+n)\rho^{\alpha+n+1}}\left[\frac{\Gamma(\alpha+n+1)}{\beta^{\alpha}}\gamma\left(\alpha,\beta T_c\right)-\sum_{k=0}^{\infty}\frac{(-1)^k(\rho T_{\mathrm{c}})^{\alpha+n+k+1}}{k!\,(\alpha+n+k+1)}B\left(\alpha+n+k+2,\alpha\right)\right.$$
$$\left.\times\, T_{\mathrm{c}}^{\alpha}\,{}_1F_1\left(\alpha;2\alpha+n+k+2;-\beta T_{\mathrm{c}}\right)\right]+\frac{\rho}{(\beta+\rho\alpha)\Gamma(\alpha)}\left\{\alpha\gamma(\alpha,\beta T_{\mathrm{c}})-\sum_{n=0}^{\infty}\frac{(-\beta T_{\mathrm{c}})^{2\alpha+n+1}}{n!\Gamma(\alpha)(\alpha+n+1)}B(\alpha+n+2,\alpha)\right.$$
$$\times{}_1F_1(\alpha;2\alpha+n+2;-\beta T_{\mathrm{c}})-(\beta T_{\mathrm{c}})^{\alpha+1}B(\alpha,2)T_{\mathrm{c}}^{\alpha}\,{}_1F_1(\alpha;\alpha+2;-\beta T_{\mathrm{c}})$$
$$\left.+\sum_{n=0}^{\infty}\frac{(-\beta T_{\mathrm{c}})^{2\alpha+n+1}}{n!\Gamma(\alpha)(\alpha+n)}B(\alpha,\alpha+n+2)\,{}_1F_1(\alpha;2\alpha+n+2;\beta T_{\mathrm{c}})\right\}+\frac{\Gamma(\alpha,\beta T_{\mathrm{c}})}{\Gamma(\alpha)}. \tag{4.11}$$

---

i.e., the probability that the AoI is being larger than a target AoI v. Then, P_v is given by [7]

$$P_v = \frac{\mathbb{E}[T_k^v]}{\mathbb{E}[T_k]}, \tag{4.9}$$

where T_k^v is the time duration of the AoI being larger than v between the update instants U_{k-1} and U_k, which can be defined as

$$\begin{aligned}T_k^v &= \min\left\{\left(\mathrm{PAoI}_k - v\right)^+, T_k\right\}\\ &= \min\left\{\left(X_{k-1}+X_k+T_{\mathrm{int}}+T_{\mathrm{tra}}-v\right)^+, X_k+T_{\mathrm{int}}\right\},\end{aligned} \tag{4.10}$$

where $(\cdot)^+ = \max(0,\ \cdot)$. We now obtain P_v in HeMN in the following theorem.

Theorem 1. In HeMN, the AoI violation probability P_v is given by (4.11) on the top of this page.

Proof. In (4.9), the expectation of T_k^v is given by

$$\mathbb{E}[T_k^v] = \int_0^{\infty}\mathbb{P}[T_k^v \geq a]da. \tag{4.12}$$

Using (4.10) and (4.12), $\mathbb{E}[T_k^v]$ can be represented by

$$\begin{aligned}\mathbb{E}[T_k^v] = &\int_0^{T_{\mathrm{c}}}\int_0^{\infty}\mathbb{P}\left[x+X_k+T_{\mathrm{int}}-T_{\mathrm{c}}\geq a\right]f_{X_{k-1}}(x)\ dadx\\ &+\int_{T_{\mathrm{c}}}^{\infty}\int_0^{\infty}\mathbb{P}[X_k+T_{\mathrm{int}}\geq a]f_{X_{k-1}}(x)\ dadx,\end{aligned} \tag{4.13}$$

where $f_{X_{k-1}}(x)$ is in (3.2), and $T_{\mathrm{c}} = v - T_{\mathrm{tra}}$. In (4.13), $\mathbb{P}\left[x+X_k+T_{\mathrm{int}}-T_{\mathrm{c}}\geq a\right]$ can be given by

$$\begin{aligned}&\mathbb{P}\left[T_{\mathrm{int}}\geq a+T_{\mathrm{c}}-x-X_k\right]\\ &=\int_0^{\infty}\mathbb{P}\left[T_{\mathrm{int}}\geq a+T_{\mathrm{c}}-x-w|X_k=w\right]f_{X_k}(w)dw\\ &\overset{(a)}{=}\int_0^{a+T_{\mathrm{c}}-x}e^{-\rho(a+T_{\mathrm{c}}-x-w)}f_{X_k}(w)dw+\int_{a+T_{\mathrm{c}}-x}^{\infty}f_{X_k}(w)dw\\ &=\frac{\beta^{\alpha}e^{-\rho(a+T_{\mathrm{c}}-x)}}{\Gamma(\alpha)}\frac{\gamma(\alpha,(\beta-\rho)(a+T_{\mathrm{c}}-x))}{(\beta-\rho)^{\alpha}}+\frac{\Gamma(\alpha,\beta(a+T_{\mathrm{c}}-x))}{\Gamma(\alpha)},\end{aligned} \tag{4.14}$$

where (a) is obtained from the fact that $\mathbb{P}\left[T_{\text{int}} \geq a+T_{\text{c}}-x-X_k|X_k\right]$ is always one when X_k is larger than $a+T_{\text{c}}-x$ and the exponential distribution of T_{int}. In (4.14), $\gamma(\cdot,\cdot)$ and $\Gamma(\cdot,\cdot)$ are the incomplete gamma functions, given by

$$\gamma(\alpha,x)=\int_0^x t^{\alpha-1}e^{-t}dt,\ \Gamma(\alpha,x)=\int_x^\infty t^{\alpha-1}e^{-t}dt. \tag{4.15}$$

Using (4.14), the inner integral of the first term in (4.13) can be obtained as

$$\begin{aligned}
&\int_0^\infty \mathbb{P}\left[x+X_k+T_{\text{int}}-T_{\text{c}} \geq a\right]da \\
&= \int_0^\infty \left[\frac{\beta^\alpha e^{-\rho(a+T_{\text{c}}-x)}}{\Gamma(\alpha)}\frac{\gamma\left(\alpha,(\beta-\rho)\left(a+T_{\text{c}}-x\right)\right)}{(\beta-\rho)^\alpha}+\frac{\Gamma\left(\alpha,\beta\left(a+T_{\text{c}}-x\right)\right)}{\Gamma(\alpha)}\right]da \\
&\overset{(a)}{=} \frac{\beta^\alpha}{\Gamma(\alpha)}\sum_{n=0}^{\infty}\frac{(\rho-\beta)^n}{n!\,(\alpha+n)}\int_0^\infty (a+T_{\text{c}}-x)^{\alpha+n}\,e^{-\rho(a+T_{\text{c}}-x)}da+\frac{1}{\Gamma(\alpha)}\int_0^\infty\int_{\beta(a+T_{\text{c}}-x)}^\infty t^{\alpha-1}e^{-t}dtda \\
&= \underbrace{\frac{\beta^\alpha}{\Gamma(\alpha)}\sum_{n=0}^{\infty}\frac{(\rho-\beta)^n}{n!\,(\alpha+n)}\frac{\Gamma\left(\alpha+n+1,\rho\left(T_{\text{c}}-x\right)\right)}{\rho^{\alpha+n+1}}}_{f_1(x)}+\underbrace{\frac{\Gamma\left(\alpha+1,\beta\left(T_{\text{c}}-x\right)\right)}{\beta\Gamma(\alpha)}}_{f_2(x)}+\underbrace{\frac{(x-T_{\text{c}})}{\Gamma(\alpha)}\Gamma\left(\alpha,\beta\left(T_{\text{c}}-x\right)\right)}_{f_3(x)},
\end{aligned} \tag{4.16}$$

where (a) is from the fact that lower incomplete Gamma function $\gamma(\alpha,x)$ can be represented as [31, eq. 8.354-1]

$$\gamma(\alpha,x)=\sum_{n=0}^{\infty}\frac{(-1)^n x^{\alpha+n}}{n!(\alpha+n)}. \tag{4.17}$$

Using (4.16), the first term in (4.13) can be represented as

$$\begin{aligned}
&\int_0^{T_{\text{c}}}\int_0^\infty \mathbb{P}\left[x+X_k+T_{\text{int}}-T_{\text{c}} \geq a\right] f_{X_{k-1}}(x)\ dadx \\
&= \int_0^{T_{\text{c}}} \left\{f_1(x)+f_2(x)+f_3(x)\right\} f_{X_{k-1}}(x)dx,
\end{aligned} \tag{4.18}$$

where $f_i(x), i=1,2,3$ are defined in (4.16). In (4.18), the first term can be given by

$$\begin{aligned}
&\int_0^{T_{\text{c}}} f_1(x)f_{X_{k-1}}(x)dx \\
&\overset{(a)}{=} \frac{\beta^{2\alpha}}{\Gamma(\alpha)^2}\sum_{n=0}^{\infty}\frac{(\rho-\beta)^n}{n!\,(\alpha+n)\,\rho^{\alpha+n+1}}\int_0^{T_{\text{c}}}\left[\Gamma\left(\alpha+n+1\right)-\sum_{k=0}^{\infty}\frac{(-1)^k\left\{\rho\left(T_{\text{c}}-x\right)\right\}^{\alpha+n+k+1}}{k!\,(\alpha+n+k+1)}\right]x^{\alpha-1}e^{-\beta x}dx \\
&\overset{(b)}{=} \frac{\beta^{2\alpha}}{\Gamma(\alpha)^2}\sum_{n=0}^{\infty}\frac{(\rho-\beta)^n}{n!\,(\alpha+n)\,\rho^{\alpha+n+1}}\left[\frac{\Gamma\left(\alpha+n+1\right)}{\beta^\alpha}\gamma\left(\alpha,\beta T_{\text{c}}\right)-\sum_{k=0}^{\infty}\frac{(-1)^k(\rho T_{\text{c}})^{\alpha+n+k+1}}{k!\,(\alpha+n+k+1)}T_{\text{c}}^\alpha B\left(\alpha+n+k+2,\alpha\right)\right. \\
&\qquad\left.\times\, {}_1F_1\left(\alpha;2\alpha+n+k+2;\beta T_{\text{c}}\right)\right],
\end{aligned} \tag{4.19}$$

where $B(\cdot,\cdot)$ is the beta function and ${}_1F_1(\cdot\,;\cdot\,;\cdot)$ is the confluent hypergeometric function. The derivation of (a) is obtained since $\Gamma(\alpha,x)=\Gamma(\alpha)-\gamma(\alpha,x)$ and (b) is from [31, eq. 3.383-1]. Similarly, in (4.18), the second term can be represented by

$$\begin{aligned}
&\int_0^{T_\mathrm{c}} f_2(x) f_{X_{k-1}}(x)dx \\
&= \frac{\beta^{2\alpha}}{\Gamma(\alpha)^2}\int_0^{T_\mathrm{c}}\left[\Gamma(\alpha+1) - \sum_{n=0}^{\infty}\frac{(-\beta)^n (T_\mathrm{c}-x)^{\alpha+n+1}}{n!\,(\alpha+n+1)}\right]x^{\alpha-1}e^{-\beta x}dx \\
&= \frac{\alpha\gamma(\alpha,\beta T_\mathrm{c})}{\beta\Gamma(\alpha)} - \frac{T_\mathrm{c}}{\Gamma(\alpha)^2}\sum_{n=0}^{\infty}\frac{(-1)^n(\beta T_\mathrm{c})^{2\alpha+n}}{n!\,(\alpha+n+1)}B(\alpha+n+2,\alpha)\,{}_1F_1(\alpha;2\alpha+n+2;-\beta T_\mathrm{c}). \qquad (4.20)
\end{aligned}$$

The third term in (4.18) is given by

$$\begin{aligned}
&\int_0^{T_\mathrm{c}} f_3(x) f_{X_{k-1}}(x)dx \\
&\overset{(a)}{=} -\frac{\beta^{\alpha}}{\Gamma(\alpha)^2}\int_0^{T_\mathrm{c}} k\Gamma(\alpha,\beta k)(T_\mathrm{c}-k)^{\alpha-1}e^{-\beta(T_\mathrm{c}-k)}dk \\
&\overset{(b)}{=} -\frac{\beta^{\alpha}}{\Gamma(\alpha)^2}\int_0^{T_\mathrm{c}}\left\{\Gamma(\alpha) - \sum_{n=0}^{\infty}\frac{(-1)^n(\beta k)^{\alpha+n}}{n!(\alpha+n)}\right\}\times k(T_\mathrm{c}-k)^{\alpha-1}e^{-\beta(T_\mathrm{c}-k)}dk \\
&\overset{(c)}{=} -\frac{T_\mathrm{c}(\beta T_\mathrm{c})^{\alpha}e^{-\beta T_\mathrm{c}}}{\Gamma(\alpha)}B(\alpha,2)\,{}_1F_1(2;\alpha+2;\beta T_\mathrm{c}) + \frac{T_\mathrm{c}e^{-\beta T_\mathrm{c}}}{\Gamma(\alpha)^2}\sum_{n=0}^{\infty}\frac{(-1)^n(\beta T_\mathrm{c})^{2\alpha+n}}{n!(\alpha+n)}B(\alpha,\alpha+n+2) \\
&\quad \times {}_1F_1(\alpha+n+2;2\alpha+n+2;\beta T_\mathrm{c}) \\
&\overset{(d)}{=} -\frac{T_\mathrm{c}(\beta T_\mathrm{c})^{\alpha}}{\Gamma(\alpha)}B(\alpha,2)\,{}_1F_1(\alpha;\alpha+2;-\beta T_\mathrm{c}) + \frac{T_\mathrm{c}}{\Gamma(\alpha)^2}\sum_{n=0}^{\infty}\frac{(-1)^n(\beta T_\mathrm{c})^{2\alpha+n}}{n!(\alpha+n)}B(\alpha,\alpha+n+2) \\
&\quad \times {}_1F_1(\alpha;2\alpha+n+2;-\beta T_\mathrm{c}), \qquad (4.21)
\end{aligned}$$

where (a) is obtained by substituting k for $T_\mathrm{c}-x$, (b) is from (4.17), and (c) is obtained by the similar steps, which are used in (4.19). In (d), it is simplified using ${}_1F_1(a;b;z) = e^z\,{}_1F_1(b-a;b;-z)$ in [31, eq. 9.212-1].

Now, we derive the second term of (4.13). In the integral range of a, $X_k + T_\mathrm{int} \geq 0$ holds. Hence, we have

$$\begin{aligned}
&\int_{T_\mathrm{c}}^{\infty}\int_0^{\infty}\mathbb{P}[X_k+T_\mathrm{int}\geq a]da f_{X_{k-1}}(x)dx \\
&\overset{(a)}{=} (\mathbb{E}[X_k]+\mathbb{E}[T_\mathrm{int}])\int_{T_\mathrm{c}}^{\infty} f_{X_{k-1}}(x)dx \\
&\overset{(b)}{=} \left(\frac{\alpha}{\beta}+\frac{1}{\rho}\right)\frac{\Gamma(\alpha,\beta T_\mathrm{c})}{\Gamma(\alpha)}, \qquad (4.22)
\end{aligned}$$

where (a) is obtained since X_k and T_int are independent and (b) is from the fact that X_k and T_int are the gamma and exponential random variables respectively.

Finally, $\mathbb{E}[T_k^v]$ is the summation of (4.19), (4.20), (4.21), and (4.22). Note that the $\mathbb{E}[T_k] = \mathbb{E}[X_k + T_\mathrm{int}] = \frac{\alpha}{\beta} + \frac{1}{\rho}$. Therefore, we obtain P_v by the ratio of $\mathbb{E}[T_k^v]$ and $\mathbb{E}[T_k]$ as (4.11). □

We can obtain the simplified expression of P_v in the following corollary for the special case that the shape parameter α is an integer.

Corollary 1. The AoI violation probability P_v with an integer shape parameter α can be given by P_v

$=$

$$\frac{\beta^{2\alpha+1}e^{-\rho T_c}\gamma\left(\alpha,T_c\left(\beta-\rho\right)\right)}{\left(\alpha\rho+\beta\right)\left(\beta-\rho\right)^{2\alpha}\Gamma(\alpha)}+\frac{\rho}{\alpha\rho+\beta}\sum_{m=0}^{\alpha-1}\sum_{k=0}^{m}\frac{(\beta T_c)^{\alpha+k}}{\Gamma(\alpha+k+1)}\times e^{-\beta T_c}\left\{1-(\rho-\beta)^{m-\alpha}\right\}$$
$$+\frac{\Gamma(\alpha,\beta T_c)}{\Gamma(\alpha)}. \tag{4.23}$$

Proof. The incomplete gamma functions, $\gamma(\alpha,x)$ and $\Gamma(\alpha,x)$, can be represented in finite series when a shape parameter is a positive integer value [31, eq. 3.351-1, 2].

$$\gamma(\alpha,x)=\Gamma(\alpha)\left(1-\sum_{n=0}^{\alpha-1}\frac{x^n e^{-x}}{n!}\right),\Gamma(\alpha,x)=\Gamma(\alpha)\sum_{n=0}^{\alpha-1}\frac{x^n e^{-x}}{n!}. \tag{4.24}$$

Using (4.24), $\mathbb{P}[T_{\mathrm{int}}\geq a+T_{\mathrm{c}}-x-X_k]$ in (4.14) can be represented as

$$\begin{aligned}&\mathbb{P}\left[T_{\mathrm{int}}\geq a+T_{\mathrm{c}}-x-X_k\right]\\&=\frac{\beta^{\alpha}e^{-\rho(a+T_c-x)}}{(\beta-\rho)^{\alpha}}-\frac{\beta^{\alpha}}{(\beta-\rho)^{\alpha}}\sum_{m=0}^{\alpha-1}\frac{(\beta-\rho)^m}{m!}\left(a+T_c-x\right)^m e^{-\beta(a+T_c-x)}\\&\quad+\sum_{m=0}^{\alpha-1}\frac{\beta^m}{m!}\left(a+T_c-x\right)^m e^{-\beta(a+T_c-x)}.\end{aligned} \tag{4.25}$$

Using (4.14), the inner integral of the first term in (4.13) can be obtained as

$$\begin{aligned}&\int_0^{\infty}\mathbb{P}\left[T_{\mathrm{int}}\geq a+T_{\mathrm{c}}-x-X_k\right]da\\&=\int_0^{\infty}\left[\frac{\beta^{\alpha}e^{-\rho(a+T_c-x)}}{(\beta-\rho)^{\alpha}}-\left\{\sum_{m=0}^{\alpha-1}\left(\frac{\beta}{(\beta-\rho)}\right)^{\alpha}\frac{(\beta-\rho)^m}{m!}-\frac{\beta^m}{m!}\right\}\times\left(a+T_c-x\right)^m e^{-\beta(a+T_c-x)}\right]da\\&=\frac{\beta^{\alpha}e^{-\rho(T_c-x)}}{\rho\left(\beta-\rho\right)^{\alpha}}-\sum_{m=0}^{\alpha-1}\frac{\Gamma\left(m+1,\beta\left(T_c-x\right)\right)}{\beta m!}\left\{1-(1-\rho/\beta)^{m-\alpha}\right\},\end{aligned} \tag{4.26}$$

where the last equation is obtained by substituting k for $a+T_{\mathrm{c}}-x$ and (4.15). Using (4.26), the first term in (4.13) can be obtained by

$$\begin{aligned}&\int_0^{T_{\mathrm{c}}}\int_0^{\infty}\mathbb{P}\left[T_{\mathrm{int}}\geq a+T_{\mathrm{c}}-x-X_k\right]f_{X_{k-1}}(x)\ dadx\\&=\int_0^{T_{\mathrm{c}}}\left[\frac{\beta^{\alpha}e^{-\rho(T_c-x)}}{\rho\left(\beta-\rho\right)^{\alpha}}-\sum_{m=0}^{\alpha-1}\frac{\Gamma\left(m+1,\beta\left(T_c-x\right)\right)}{\beta m!}\left\{1-(1-\rho/\beta)^{m-\alpha}\right\}f_{X_{k-1}}(x)\ dx\right]\\&\overset{(a)}{=}\frac{e^{-\rho T_c}\beta^{2\alpha}\gamma\left(\alpha,T_c\left(\beta-\rho\right)\right)}{\rho\Gamma(\alpha)\left(\beta-\rho\right)^{2\alpha}}+\sum_{m=0}^{\alpha-1}\sum_{k=0}^{m}\frac{\beta^{\alpha+k-1}T_c^{\alpha+k}}{\Gamma(\alpha+k+1)}e^{-\beta T_c}\left\{1-(1-\rho/\beta)^{m-\alpha}\right\},\end{aligned} \tag{4.27}$$

where (a) is from the definition of a lower incomplete gamma function and [31, eq. 3.191-1] and from the fact that a beta function $B(a,b)$ is the same as $\Gamma(a)\Gamma(b)/\Gamma(a+b)$ [31, eq. 8.384-1]. From (4.9), (4.13), (4.22), and (4.27), P_v with an integer shape parameter can be obtained as (4.23).

□

In Fig. 4.2, we compare the analytical results of the special cases from Corollary 1 as a function of

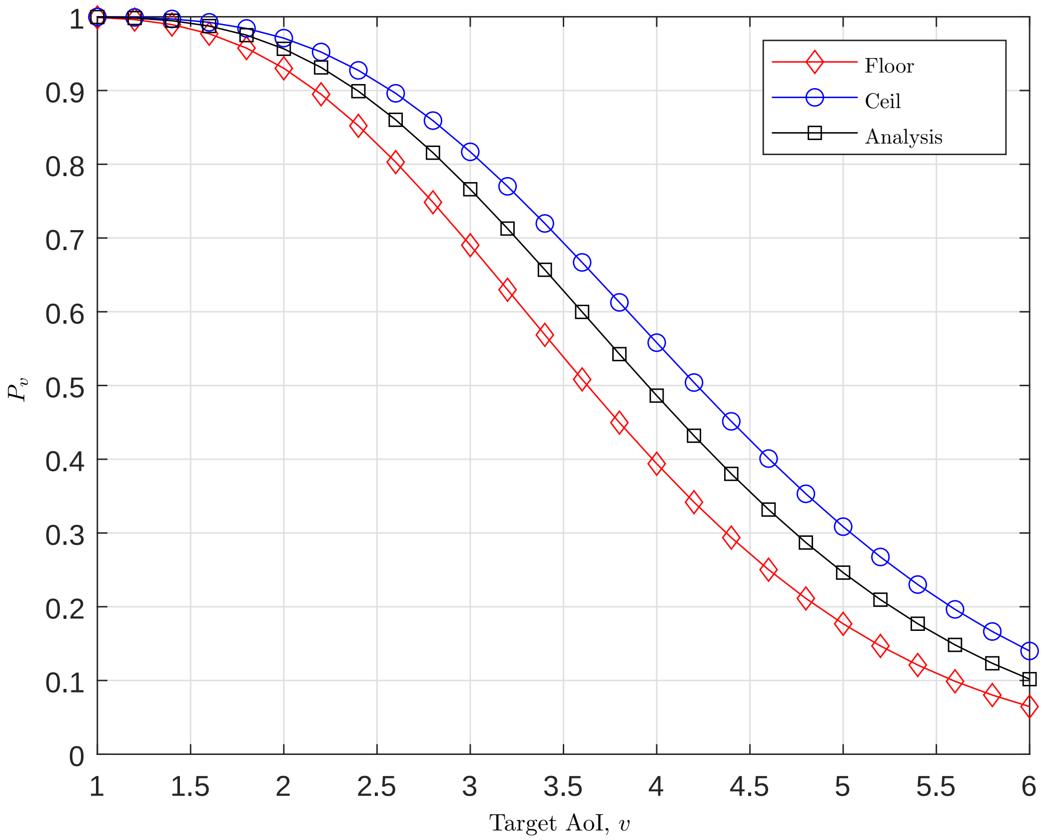

Figure 4.2: AoI violation probability P_v as a function of a target AoI v for different shape parameters.

v for a target STP $\zeta = 0.5$, block size $\hat{B} = 20$, and timeout $\hat{T} = 3$. The shape parameter ($\alpha = 5.55$) is approximated to integers by the ceil and the floor function. As shown in Fig. 4.2, the special cases can be a lower or an upper bound to the results of Theorem 1. This is from the fact that a complementary cumulative distribution function (CCDF) of a consensus latency can be upper bounded by the one with a higher shape parameter, and vice versa. Since $\alpha = 5.55$ is closer to the output of the ceil function, the approximated results by the ceil function is tighter than the floor function. P_v in Corollary 1 can also be used for approximation of the result in Theorem 1 to reduce the computational complexity.

The PAoI represents the largest value of staleness of status in update interval. Thus, the PAoI violation probability can be useful if system requirements are on the extreme value of status, which is the tail of the PAoI distribution. We define $\hat{P}_v = \mathbb{P}[\text{PAoI} \geq v]$, i.e., the probability that the PAoI is being larger than v. We then present $\hat{P}_v$ as follows.

Lemma 2. In HeMN, the PAoI violation probability $\hat{P}_v$ is given by $\hat{P}_v =$

$$1 - \frac{\beta^{2\alpha}}{\Gamma(\alpha)^2} \sum_{n=0}^{\infty} \sum_{k=0}^{\infty} \frac{T_c^{2\alpha+n+k}}{n!k!(\alpha+n)} B(\alpha+n+1, \alpha+k) \left\{(-\beta)^{n+k} - e^{-\rho T_c} (\rho-\beta)^{n+k}\right\} \tag{4.28}$$

Proof. Using (4.2), the CDF of the PAoI_k is given by

$$F_{\text{PAoI}_k}(v) = \mathbb{P}[T_{\text{eff},k} + T_{\text{tot},k} \leq v], \tag{4.29}$$

where v is the target PAoI. From (3.1) and (4.1), $\mathbb{P}[T_{\text{eff},k} + T_{\text{tot},k} \leq t]$ is the same as $\mathbb{P}[X_{k-1} + X_k + T_{\text{int}} + T_{\text{tra}} \leq v]$ given by

$$\begin{aligned} F_{\text{PAoI}_k}(v) &= \mathbb{P}[X_{k-1} + X_k + T_{\text{int}} + T_{\text{tra}} \leq v] \\ &= \int_0^{v-T_{\text{tra}}} \mathbb{P}[x + X_k + T_{\text{int}} \leq v - T_{\text{tra}}] f_{X_{k-1}}(x) dx \\ &= \int_0^{v-T_{\text{tra}}} \int_0^{v-T_{\text{tra}}-x} \left\{1 - e^{-\rho\left(v - T_{\text{tra}} - x - x'\right)}\right\} f_{X_k}(x') f_{X_{k-1}}(x) dx' dx \end{aligned} \tag{4.30}$$

By using (4.15), $F_{\text{PAoI}_k}(v)$ in (4.30) can be given by

$$F_{\text{PAoI}_k}(v) = \frac{1}{\Gamma(\alpha)} \int_0^{T_c} \left[\gamma\left(\alpha, \beta\left(T_c - x\right)\right) - \frac{\beta^\alpha e^{-\rho(T_c - x)}}{(\beta-\rho)^\alpha} \gamma(\alpha, (\beta-\rho)(T_c - x))\right] f_{X_{k-1}}(x) dx, \tag{4.31}$$

where $T_c = v - T_{\text{tra}}$. Using the Taylor series of the $\exp(-\beta(T_c - x))$ and (4.17), $F_{\text{PAoI}_k}(t)$ in (4.31) is given by

$$\begin{aligned} &F_{\text{PAoI}_k}(v) \\ &= \frac{\beta^{2\alpha}}{\Gamma(\alpha)^2} \sum_{n=0}^{\infty} \sum_{k=0}^{\infty} \left[\frac{1}{n!k!\,(\alpha+n)} \int_0^{T_c} (T_c - x)^n \, x^{\alpha+k-1} \left\{(-\beta)^{n+k} - e^{-\rho T_c} \, (\rho-\beta)^{n+k} (T_c - x)^\alpha dx\right\}\right]. \end{aligned} \tag{4.32}$$

Using the equation in [31, eq. 3.191-1] and (3.2), $F_{\mathrm{PAoI}_k}(t)$ in (4.32) is given by.

$$
\begin{aligned}
&F_{\mathrm{PAoI}_k}(v) \\
&= \frac{\beta^{2\alpha}}{\Gamma(\alpha)^2} \sum_{n=0}^{\infty} \sum_{k=0}^{\infty} \frac{T_c^{2\alpha+n+k}}{n!k!(\alpha+n)} B(\alpha+n+1, \alpha+k) \left\{(-\beta)^{n+k} - e^{-\rho T_c} (\rho-\beta)^{n+k}\right\}.
\end{aligned} \tag{4.33}
$$

By taking a complementary (4.33), we obtain $\hat{P}_v$ as (4.28).

□

The analysis of the PAoI can show the distribution of the worst case data freshness during update intervals. $\hat{P}_v$ can be a metric for the systems that requires strict freshness of data such as autonomous vehicular systems and health monitoring applications.

V. Numerical Results

In this section, we present the experiment results to verify the analysis of the AoI violation probability P_v and show the impact of HeMN parameters, i.e., target STP ζ, block size $\hat{B}$, and timeout $\hat{T}$, on it. We set $\rho_s = 15$, $P = 1$ W, $N_0 = -100$ dBm, $W = 1$ MHz, $D = 500$ Kb, $\lambda = 0.0001$ (BS/km^2), $\zeta = 0.6$, $\hat{B} = 20$, and $\hat{T} = 3$ as default values. We implement a HLF platform with version 1.3 [35] on one physical machine with Intel(R) Xeon W-2155 @ 3.30GHz with 16 GB of RAM. The established HLF consists of one peer and two committing peers. Note that the committing peers only verify new blocks conveyed from the ordering service. We generate the transactions to update a certain target key-value, which takes 30 percent of the whole generation. We measure the consensus latency of the generated target transactions with varying HeMN parameters. To investigate the effect of each parameter, we fit statistical distribution for the thousand transactions at different HeMN parameters. Note that we use the maximum likelihood estimation method introduced in Section 3.0.2. The accuracy of the consensus latency modeling is investigated with KS test in the following.

5.0.1 KS Test

The KS test returns the absolute value of the largest discrepancy between an empirical and theoretical cumulative distribution, which is referred to as the KS statistic [36]. The smaller the KS statistic, the more accurate modeling is. The KS test compares the KS statistic with a critical value, which is determined by the number of samples and a significance level. If the KS statistic is smaller than the critical value, it is reasonable to model empirical distribution as the theoretical distribution with the estimated parameters. From the generated transactions above, the corresponding estimated parameters and the KS statistics with a significance level of 0.01 are averaged over five runs and presented in Table 5.1 and 5.2. We also present the averaged consensus latency, standard deviation (SD) and skewness of the distribution from the experiments. Note that the critical value of KS test for 1000 samples is 0.0515.

5.0.2 Validation of Analysis

In Figures 5.1, 5.2, and 5.3, we compare the analytical results with the simulation and the experiment results with varying the HeMN parameters as a function of v. In the simulations, P_v is calculated by using the Monte Carlo method. Fig. 5.1 presents P_v with the simulation and the experiment results as

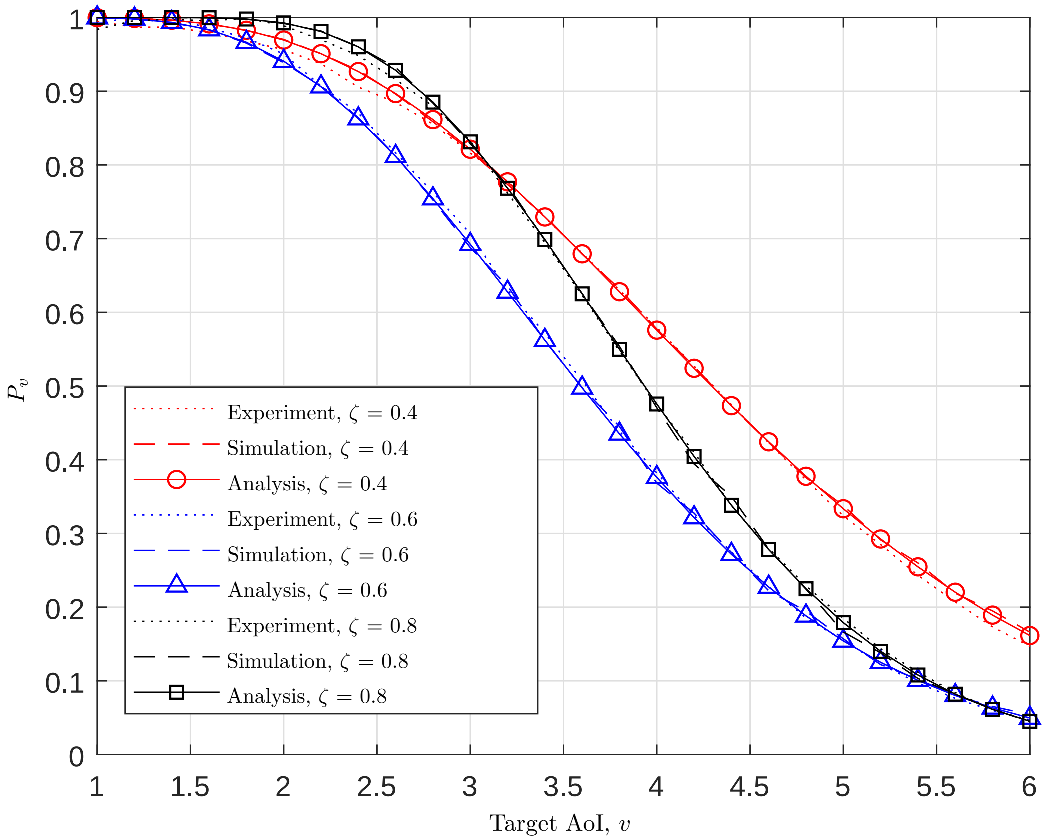

Figure 5.1: AoI violation probability P_v as a function of a target AoI v for different target STPs ζ.

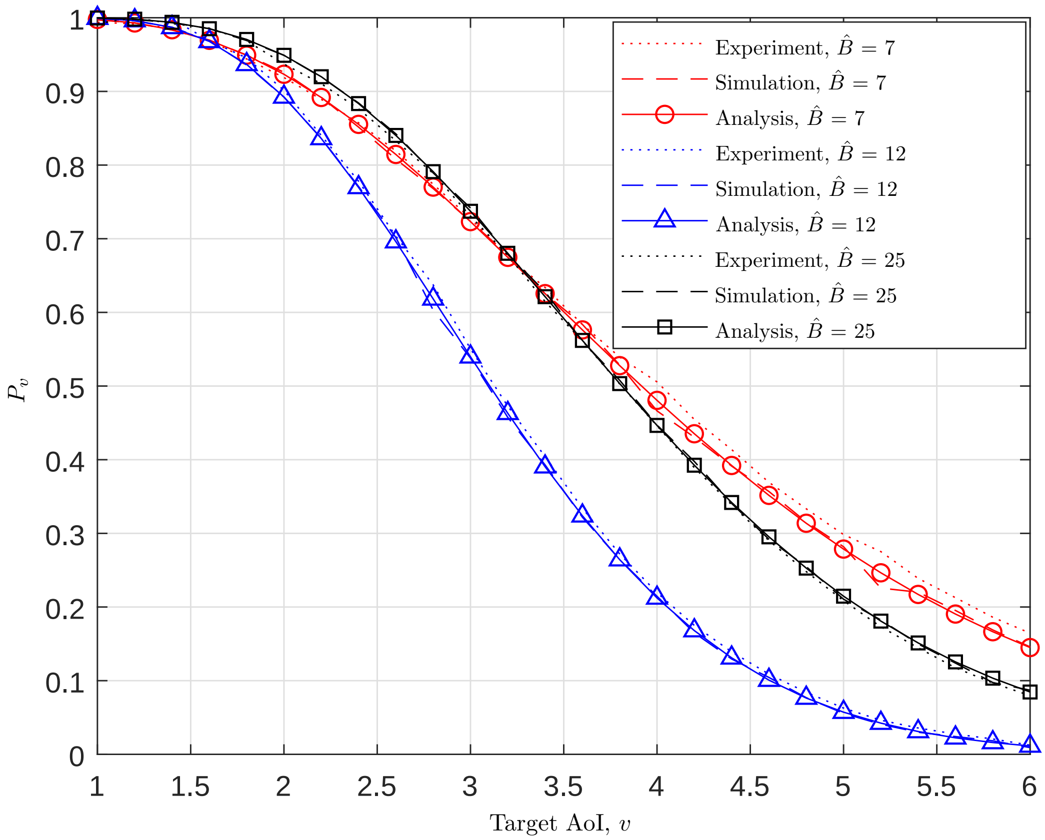

Figure 5.2: AoI violation probability P_v as a function of target AoI v for different block size $\hat{B}$.

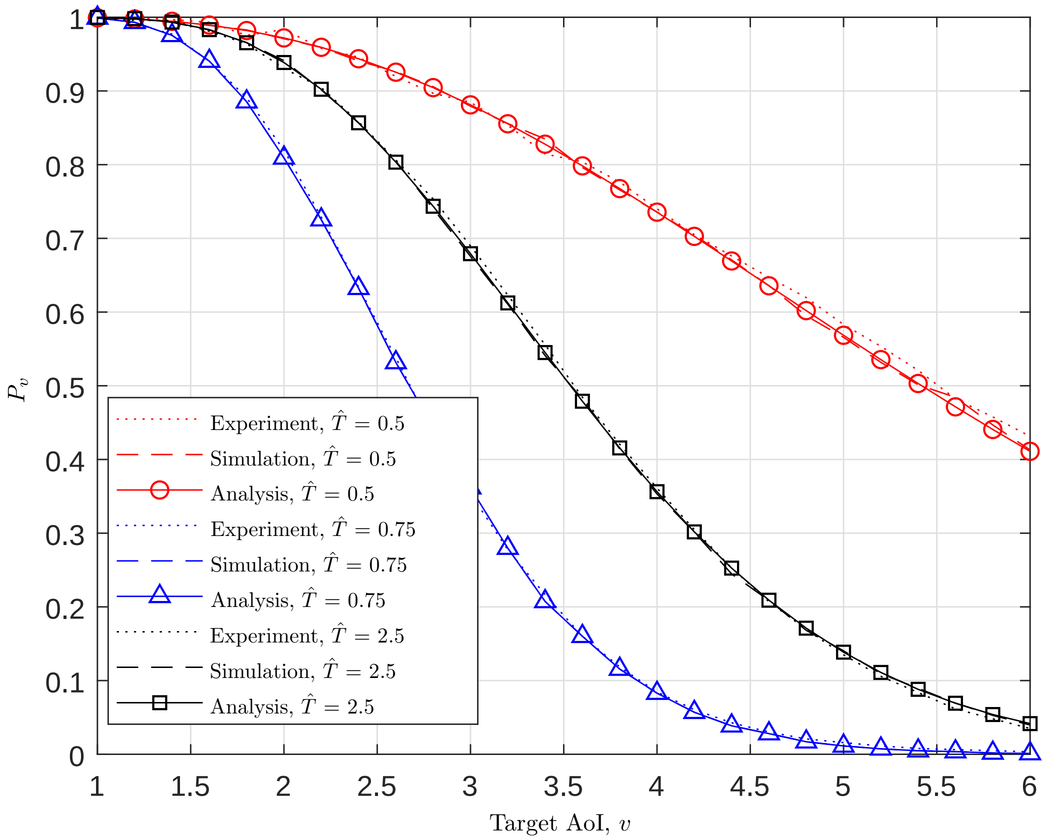

Figure 5.3: AoI violation probability P_v as a function of target AoI v for different timeout $\hat{T}$.

Table 5.1: Average estimated parameters for the Gamma distribution and the average KS statistics for varying a target STP ζ and block size $\hat{B}$.

ζ	Average estimate (α, β)	Average latency/SD	Average skewness	Average KS statistics
0.3	(5.64, 3.01)	2.42/0.95	0.093	0.0732
0.4	(5.94, 2.45)	2.42/0.92	0.086	0.0623
0.5	(5.39, 2.85)	2.17/0.87	0.095	0.0506
0.6	(5.42, 2.84)	1.90/0.76	0.097	0.0504
0.7	(7.18, 3.73)	1.92/0.67	0.071	0.0462
0.8	(7.71, 4.12)	1.87/0.63	0.066	0.0423
0.9	(7.50, 4.35)	1.73/0.60	0.068	0.0369
1.0	(6.57, 3.82)	1.76/0.76	0.085	0.0532

$\hat{B}$	Average estimate (α, β)	Average latency/SD	Average skewness	Average KS statistics
3	(1.62, 0.30)	5.71/4.03	0.342	0.0831
5	(2.90, 1.38)	1.25/2.16	0.182	0.0333
7	(4.35, 2.58)	1.70/0.85	0.121	0.0498
10	(5.24, 3.30)	1.59/0.74	0.099	0.0495
12	(5.81, 3.66)	1.58/0.63	0.074	0.0382
15	(6.95, 3.85)	1.80/0.65	0.074	0.0381
20	(5.42, 2.84)	1.90/0.76	0.097	0.0504
25	(4.85, 2.36)	2.05/0.86	0.107	0.0604

Table 5.2: Average estimated parameters for the Gamma distribution and the average KS statistics for varying a timeout $\hat{T}$.

$\hat{T}$	Average estimate (α, β)	Average latency/SD	Average skewness	Average KS statistics
0.5	(2.74, 0.89)	3.08/2.00	0.194	0.0420
0.6	(4.26, 2.04)	2.10/1.07	0.122	0.0452
0.7	(8.28, 5.40)	1.53/0.54	0..61	0.0494
0.75	(6.78, 5.19)	1.30/0.47	0.076	0.0489
1.0	(6.96, 4.65)	1.50/0.54	0.075	0.0588
1.25	(9.62, 5.37)	1.79/0.55	0.053	0.0446
1.50	(9.86, 5.20)	1.89/0.56	0.052	0.0603
2.0	(6.79, 3.62)	1.87/0.66	0.075	0.0535
2.5	(5.64, 3.01)	1.97/0.72	0.091	0.0497
3.0	(5.42, 2.84)	1.89/0.76	0.097	0.0504
3.5	(5.39, 2.85)	1.89/0.75	0.091	0.0503

a function of v for $\zeta = 0.4, 0.6$, and 0.8 at $\hat{B} = 20$, and $\hat{T} = 3$. Fig. 5.1 shows that the analytical results match the experiment results obtained from the HLF platform. Specifically, from Table 5.1, the KS statistics of $\zeta = 0.6$ and $\zeta = 0.8$ are smaller than the critical value. As can be expected, those two cases show a good match between the analytical and experiment results. Moreover, the analytical results of $\zeta = 0.4$ and the experiment results also match well even though the KS statistic of $\zeta = 0.4$ is larger than the critical value. This is from the fact that the distribution of the consensus latencies of the generated transactions and modeled distribution have similar statistical properties. Specifically, in Table 5.1, the average skewness, latency, and SD of the experiments are similar to those values calculated from the estimated parameters, which are 0.082, 2.42, and 0.98, respectively. Therefore, our analysis of the AoI can capture the actual data freshness in HeMN.

In addition, as v increases, P_v of $\zeta = 0.8$ decays faster than P_v of $\zeta = 0.4$. From (3.21), the transmission latency T_{tra} increases as ζ becomes larger. It then becomes difficult for the consensus latency to complete the status update within a short v for high ζ. Hence, as v increases, P_v of $\zeta = 0.8$

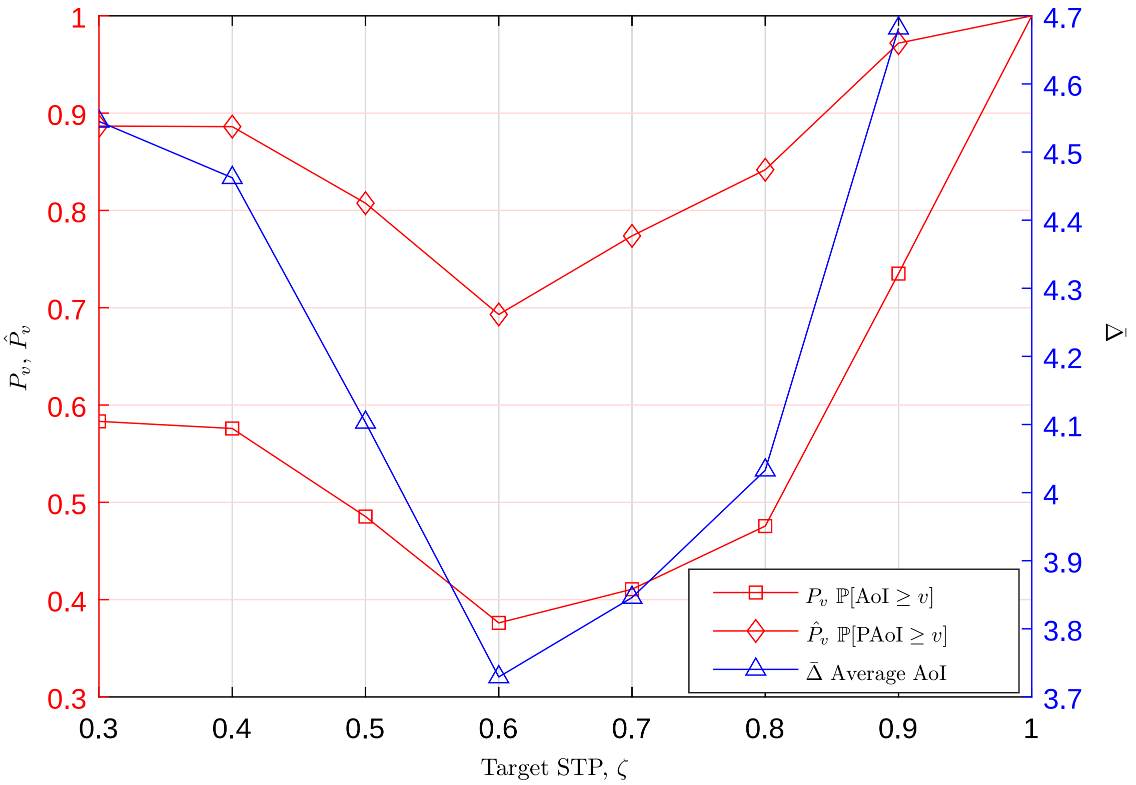

Figure 5.4: AoI violation probability P_v versus target STP ζ for the target AoI $v = 4$, block size $\hat{B} = 20$, and timeout $\hat{T} = 3$.

shows faster decay rate since it can leverage the larger number of successfully received packets than P_v of $\zeta = 0.4$.

Fig. 5.2 shows the analytical, simulation, and experiment results of P_v as a function of v for $\hat{B} = 7$, 12, and 25 at $\zeta = 0.6$ and $\hat{T} = 3$. From Fig. 5.2, we can see that the three results coincide well. For P_v of $\hat{B} = 25$, it decays faster than P_v of $\hat{B} = 7$ as v increases. As $\hat{B}$ becomes larger, the amount of time that a transaction has to wait in a block also increases. The case of $\hat{B} = 25$ hardly completes its status update without violation for a small v. Thus, as v becomes more relaxed, P_v of $\zeta = 0.8$ becomes lower than P_v of $\zeta = 0.4$ since the time for the validation phase to commit block of size N is always lesser than to commit m blocks of size $\frac{N}{m}$ for $m \geq 1$ [37].

Fig. 5.3 presents the three results of P_v as a function of v for $\hat{T} = 0.5, 0.75$, and 2.5 at $\zeta = 0.6$ and $\hat{B} = 20$. Similarly, we observe that the analytical and experiment results also show a good match.

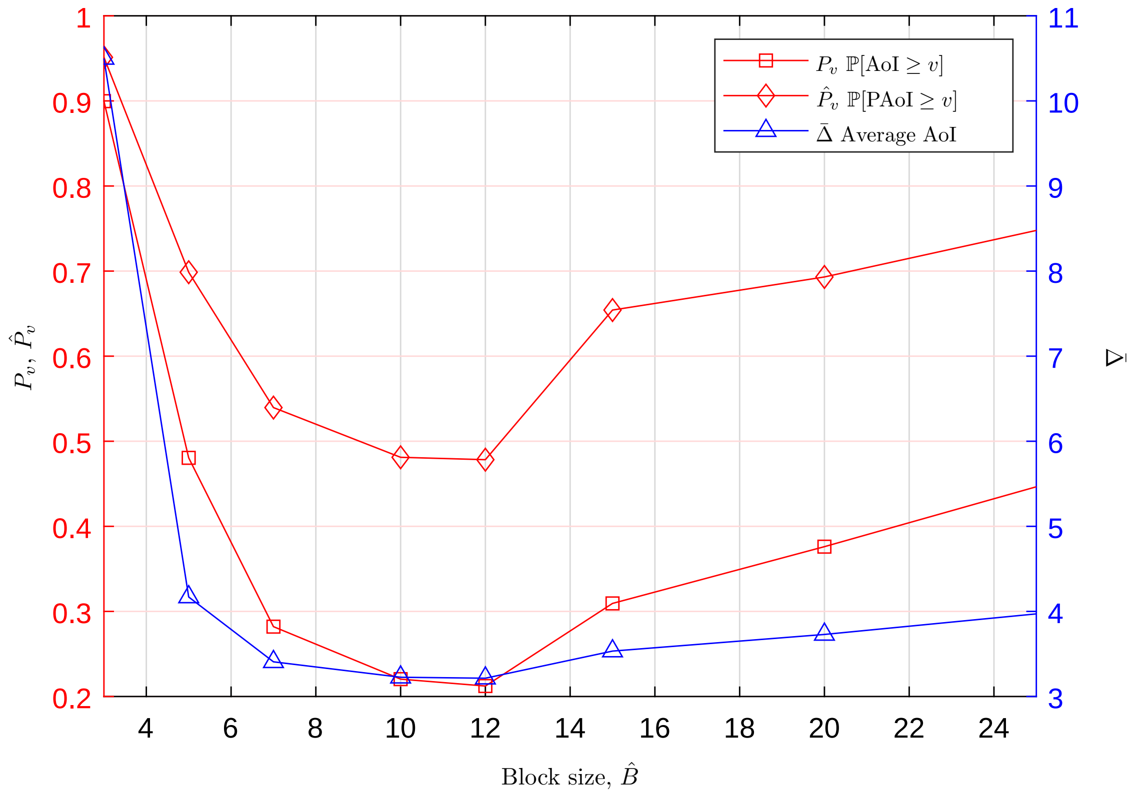

Figure 5.5: AoI violation probability P_v versus block size $\hat{B}$ for the target AoI $v = 4$, target STP $\zeta = 0.6$, and timeout $\hat{T} = 3$.

5.0.3 Impact of HeMN Parameters

Figure 5.4 shows P_v, $\hat{P}_v$, and $\bar{\Delta}$ for different values of ζ with $v = 4$, $\hat{B} = 20$, and $\hat{T} = 3$. We compute the three values at each ζ from the estimated parameters. As shown in Fig. 5.4, ζ and the every three metrics have a trade-off relationship. In specific, when ζ is small, P_v also becomes small due to the frequent outages of packets. For ζ, increasing it leads to decreased P_v. Since ζ can guarantee a certain level of STP, its increment results in more successfully received packets for the status update. However, after a certain point of ζ, as ζ becomes larger, P_v also increases. This is from the fact that large ζ not only guarantees a reliable transmission but also increases T_{tra} as shown in (3.21). For this reason, it becomes difficult for the consensus process to be completed within v at high ζ. Hence, the optimal ζ exists for minimizing P_v. For the same reason, both $\hat{P}_v$ and $\bar{\Delta}$ show a similar trend versus ζ. Therefore, a source can adopt the strategy that it reduces ζ to achieve fresh status stored in ledgers at the expense of outages.

Figure 5.5 presents P_v, $\hat{P}_v$, and $\bar{\Delta}$ for different values of $\hat{B}$ with $v = 4$, $\zeta = 0.6$, and $\hat{T} = 3$. The

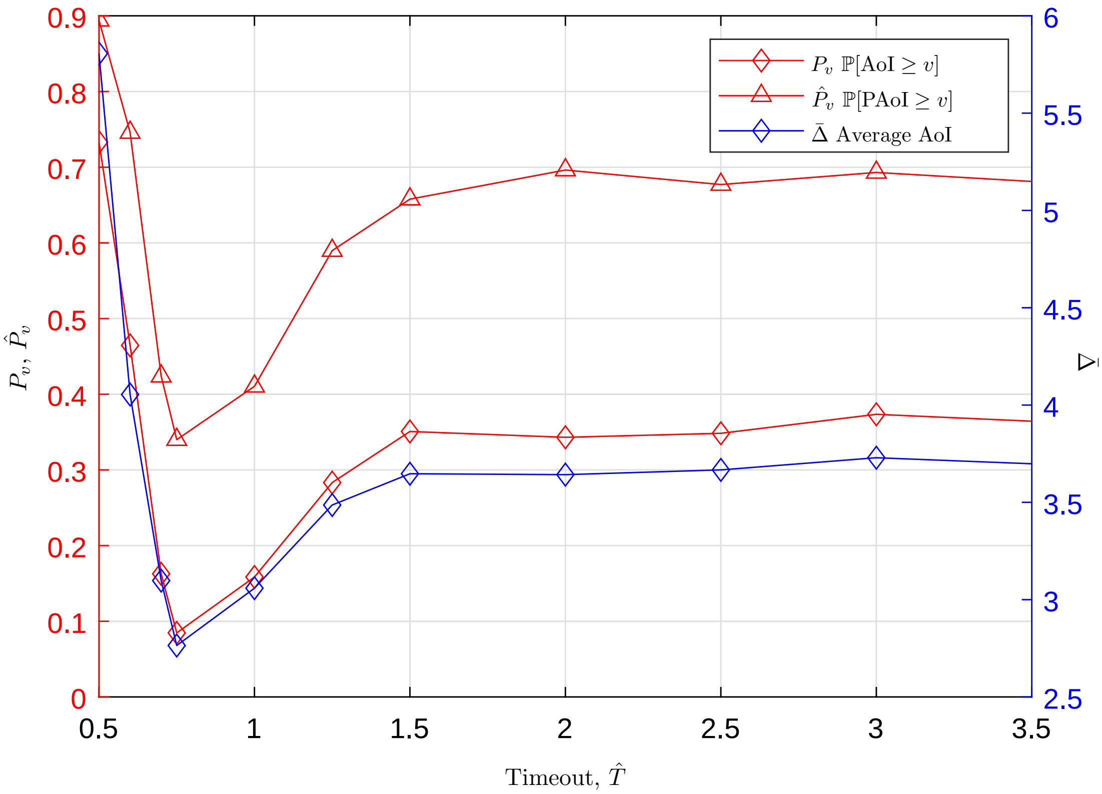

Figure 5.6: AoI violation probability P_v versus timeout $\hat{T}$ for the target AoI $v = 4$, target AoI $\zeta = 0.6$, and block size $\hat{B} = 20$.

three values are calculated from the estimated parameters corresponding to the samples at each $\hat{B}$. As depicted in Fig. 5.5, they show a similar trend versus $\hat{B}$. P_v becomes larger at smaller $\hat{B}$ since the block generation rate exceeds the block commitment rate at a certain point. For small $\hat{B}$, the blocks generation rate in the ordering phase is beyond the capability of peers in the validation phase. It takes more time for peers to validate a given number of transactions when the transactions are stored in smaller blocks compared with larger blocks [37]. In consequence, the consensus latency becomes larger if $\hat{B}$ is set to be too small. As $\hat{B}$ increases, P_v decreases due to the reduced amount of blocks to be committed in the validation phase. However, as $\hat{B}$ keeps increasing, P_v also becomes large since a transaction has to wait longer in the ordering phase. Therefore, we can see that $\hat{B}$ and the AoI violation probability have a trade-off relationship from Figure 5.5. Similarly, we illustrate the trend of $\hat{P}_v$ and $\bar{\Delta}$ versus $\hat{B}$.

In Figure 5.6, we present P_v, $\hat{P}_v$, and $\bar{\Delta}$ for different values of $\hat{T}$ with $v = 4$, $\zeta = 0.6$, and $\hat{B} = 20$. The results are obtained from the estimated parameters from the experiment data at each $\hat{T}$. We observe that the three values and $\hat{T}$ have a trade-off relationship. A small $\hat{T}$ (e.g., less than 0.75 seconds) makes P_v significantly increase for the similar reason from Fig. 5.5. The block generation rate of the ordering phase exceeds the service rate of the validation phase. As $\hat{T}$ increases, P_v decreases because the number of blocks transmitted from the ordering phase to the peers is reduced. However, after a certain point of $\hat{T}$, P_v increases with $\hat{T}$. This is from the fact that a transaction needs to wait longer until $\hat{T}$ expires. From Fig. 5.6, we can see that the impact of $\hat{T}$ decreases as it becomes large. If the average number of received transactions during $\hat{T}$ exceeds $\hat{B}$, i.e., $\rho_s \cdot \hat{T} \geq \hat{B}$, the effect of $\hat{T}$ almost disappears. Thus, P_v does not change at some point. For the same reason, the effect of a large $\hat{T}$ also disappears in $\hat{P}_v$ and $\bar{\Delta}$.

VI. CONCLUSIONS

In this paper, we have studied the characteristics of the AoI for HeMN. By considering both the transmission latency and the consensus latency, we present the closed-form expressions for the average AoI, the AoI violation probability and the PAoI violation probability. The special case of the AoI violation probability is also obtained, which is more computationally tractable. Further, we validate our analytical expression of the AoI violation probability through the simulations and the experiments after constructing the HLF platform. We show that the analytical results can provide the stochastic guarantee for the freshness of data in HeMN. Moreover, we investigate the effects of influential factors on the AoI violation probability in HeMN, which are the communication parameters and the HLF parameters. The experiment results show an efficacy of increasing a target AoI and a trade-off relationship between the parameters of HeMN and the AoI violation probability, which can provide some design insights into keeping data fresh. Specifically, 1) data freshness for HeMN can be generally more reliably guaranteed at the expense of increasing target AoI for larger HeMN parameters, 2) the status of the ledger can be freshly maintained when the target STP is not set to be too large, 3) the block size and the timeout can induce a lengthy consensus process, which can make the status of the ledger stale, when they are set to be too small, and 4) the optimal value of the HeMN parameters are the same for minimization of the average AoI, the AoI violation probability and the PAoI violation probability. The analysis of the AoI characteristics for HeMN can be applied to monitoring applications such as temperature monitoring systems or traffic management for vehicle systems, where freshness and integrity of information are required.

References

[1] S. Kaul, R. Yates, and M. Gruteser, “Real-time status: How often should one update?” in *Proc. IEEE Conf. on Computer Commun.*, Orlando, FL, USA, Mar. 2012, pp. 1–5.

[2] R. Yates and S. Kaul, “Real-time status updating: Multiple sources,” in *Proc. IEEE Int. Symp. on Inf. Theory*, Cambridge, MA, USA, Jul. 2012, pp. 1–5.

[3] M. Costa, M. Codreanu, and A. Enpremides, “On the age of information in status update systems with packet management,” *IEEE Trans. Inf. Theory*, vol. 62, no. 4, pp. 1897–1910, Apr. 2016.

[4] Y. Inoue, H. Masuyama, T. Takine, and T. Tanaka, “A general formula for the stationary distribution of the age of information and its application to single-server queues,” *IEEE Trans. Inf. Theory*, vol. 65, no. 12, pp. 8305–8324, Aug. 2019.

[5] J. P. Champati, H. Al-Zubaidy, and J. Gross, “Statistical guarantee optimization for age of information for the D/G/1 queue,” in *Proc. IEEE Conf. on Computer Commun.*, Mar. 2018.

[6] J. Seo and J. Choi, “On the outage probability of peak age-of-information for D/G/1 queuing systems,” *IEEE Commun. Lett.*, vol. 23, no. 6, pp. 1021–1024, 2019.

[7] J. P. Champati, H. Al-Zubaidy, and J. Gross, “On the distribution of age of information for the GI/GI/1/1 and GI/GI/1/2* systems: Exact expressions and bounds,” in *Proc. IEEE Conf. on Computer Commun.*, Paris, France, Apr. 2019, pp. 37–45.

[8] R. Devassy, G. Durisi, G. C. Ferrante, O. Simeone, and E. Uysal, “Reliable transmission of short packets through queues and noisy channels under latency and peak-age violation guarantees,” *IEEE J. Sel. Areas Commun.*, vol. 37, no. 4, pp. 721–734, 2019.

[9] M. A. Abd-Elmagid, N. Pappas, and H. S. Dhillon, “On the role of age of information in the internet of things,” *IEEE Commun. Mag.*, vol. 57, no. 12, pp. 72–77, 2019.

[10] X. Zheng, S. Zhou, Z. Jiang, and Z. Niu, “Closed-form analysis of non-linear age of information in status updates with an energy harvesting transmitter,” *IEEE Trans. Wireless Commun.*, vol. 18, no. 8, pp. 4129–4142, 2019.

[11] Y. Gu, H. Chen, Y. Zhou, Y. Li, and B. Vucetic, "Timely status update in internet of things monitoring systems: An age-energy tradeoff," *IEEE Internet Things J.*, vol. 6, no. 3, pp. 5324–5335, 2019.

[12] M. A. Khan and K. Salah, "IoT security: Review, blockchain solutions, and open challenges," *Future Generation Computer Systems*, vol. 82, pp. 395–411, 2018.

[13] L. Hang and D. Kim, "Design and implementation of an integrated IoT blockchain platform for sensing data integrity," *Sensors*, vol. 19, no. 10, p. 2228, 2019.

[14] P. Danzi, A. E. Kalør, C. Stefanović, and P. Popovski, "Delay and communication tradeoffs for blockchain systems with lightweight IoT clients," *IEEE Internet Things J.*, vol. 6, no. 2, pp. 2354–2365, 2019.

[15] M. Alaslani, F. Nawab, and B. Shihada, "Blockchain in iot systems: End-to-end delay evaluation," *IEEE Internet Things J.*, vol. 6, no. 5, pp. 8332–8344, 2019.

[16] Y. Sun, L. Zhang, G. Feng, B. Yang, B. Cao, and M. A. Imran, "Blockchain-enabled wireless internet of things: Performance analysis and optimal communication node deployment," *IEEE Internet Things J.*, vol. 6, no. 3, pp. 5791–5802, 2019.

[17] P. Danzi, A. E. Kalor, R. B. Sorensen, A. K. Hagelskjaer, L. D. Nguyen, C. Stefanovic, and P. Popovski, "Communication aspects of the integration of wireless iot devices with distributed ledger technology," *IEEE Network*, vol. 34, no. 1, pp. 47–53, 2020.

[18] A. Rovira-Suganes and A. Razi, "Optimizing the age of information for blockchain technology with applications to IoT sensors," *IEEE Commun. Lett.*, vol. 24, no. 1, pp. 183–187, Jan. 2020.

[19] E. Androulaki, A. Barger, V. Bortnikov, C. Cachin, K. Christidis, A. De Caro, D. Enyeart, C. Ferris, G. Laventman, Y. Manevich *et al.*, "Hyperledger Fabric: a distributed operating system for permissioned blockchains," in *Proc. EuroSys Conference*, 2018, pp. 1–15.

[20] S. Lee, M. Kim, J. Lee, R.-H. Hsu, and T. Q. S. Quek, "Is blockchain suitable for data freshness? – age-of-information perspective," *arXiv preprint arXiv:2006.02735*, 2020.

[21] . Ledeczi, T. Hay, P. Volgyesi, D. R. Hay, A. Nadas, and S. Jayaraman, "Wireless acoustic emission sensor network for structural monitoring," *IEEE Sensors J.*, vol. 9, no. 11, pp. 1370–1377, 2009.

[22] I. Martin, T. O'Farrell, R. Aspey, S. Edwards, T. James, P. Loskot, T. Murray, I. Rutt, N. Selmes, and T. Baugé, "A high-resolution sensor network for monitoring glacier dynamics," *IEEE Sensors J.*, vol. 14, no. 11, pp. 3926–3931, 2014.

[23] H. C. Thom, "A note on the gamma distribution," *Monthly Weather Review*, vol. 86, no. 4, pp. 117–122, 1958.

[24] N. T. Ison, A. M. Feyerherm, and L. D. Bark, "Wet period precipitation and the gamma distribution," *Journal of Applied Meteorology*, vol. 10, no. 4, pp. 658–665, 1971.

[25] J. W. Shin, J.-H. Chang, and N. S. Kim, "Statistical modeling of speech signals based on generalized gamma distribution," *IEEE Signal Process. Lett.*, vol. 12, no. 3, pp. 258–261, 2005.

[26] C. Park and J. Lee, "Mobile edge computing-enabled heterogeneous networks," *arXiv preprint arXiv:1804.07756*, 2018.

[27] L. H. Ozarow, S. Shamai, and A. D. Wyner, "Information theoretic considerations for cellular mobile radio," *IEEE Trans. Veh. Technol.*, vol. 43, no. 2, pp. 359–378, 1994.

[28] S. Singh, H. S. Dhillon, and J. G. Andrews, "Offloading in heterogeneous networks: Modeling, analysis, and design insights," *IEEE Trans. Wireless Commun.*, vol. 12, no. 5, pp. 2484–2497, 2013.

[29] T. D. Novlan, H. S. Dhillon, and J. G. Andrews, "Analytical modeling of uplink cellular networks," *IEEE Trans. Wireless Commun.*, vol. 12, no. 6, pp. 2669–2679, 2013.

[30] M. Haenggi and R. K. Ganti, *Interference in large wireless networks.* Now Publishers Inc, 2009.

[31] I. S. Gradshteyn and I. M. Ryzhik, *Table of integrals, series, and products.* Academic press, 2014.

[32] J. Zhao and R. Govindan, "Understanding packet delivery performance in dense wireless sensor networks," in *Proc. ACM SENSYS*, 2003, pp. 1–13.

[33] A. Valehi and A. Razi, "Maximizing energy efficiency of cognitive wireless sensor networks with constrained age of information," *IEEE Trans. Cogn. Commun. Netw.*, vol. 3, no. 4, pp. 643–654, 2017.

[34] Y. Sun, E. Uysal-Biyikoglu, R. D. Yates, C. E. Koksal, and N. B. Shroff, "Update or wait: How to keep your data fresh," *IEEE Trans. Inf. Theory*, vol. 63, no. 11, pp. 7492–7508, 2017.

[35] Https://github.com/hyperledger/fabric/releases/tag/v1.3.0.

[36] A. H.-S. Ang and W. H. Tang, *Probability concepts in engineering planning and design: Emphasis on application to civil and environmental engineering.* Wiley, 2007.

[37] P. Thakkar, S. Nathan, and B. Viswanathan, “Performance benchmarking and optimizing hyperledger fabric blockchain platform,” in *in Proc. IEEE Int. Symp. on Modeling, Analysis, and Simulation of Computer and Telecommunication Systems (MASCOTS)*, Milwaukee, WI, USA, Sep. 2018, pp. 1–13.

요 약 문

하이퍼레저 페브릭을 활용한 모니터링 네트워크에서 정보의 최신성 분석

Age of Information (AoI)는 정보의 최신성을 측정하기 위해 도입된 개념으로 실시간 관측 시스템과 같은 신선한 정보가 요구되는 곳에서 연구가 이루어져 왔다. 본 학위논문에서는 하이퍼레저 패브릭 블록체인을 활용한 관측 시스템 (HeMN)에서 AoI를 이용하여 정보의 최신성을 분석하였다. HeMN에서는 센서가 관측한 정보를 연결된 기지국으로 전송하여 하이퍼레저 패브릭 네트워크에 저장한다. HeMN에서의 AoI 특성을 분석하기 위해 Peak AoI의 분포와 평균 AoI를 제시하였다. 또한, 일정 수준의 최신성을 보장할 수 있는지 분석하기 위해 전송 지연 시간과 합의 지연 시간을 같이 고려하여 AoI violation 확률을 제시하였다. 도출한 수식의 검증을 위해 하이퍼레저 패브릭 네트워크를 구축하였고 실험을 통해 그 타당성을 보였다. 또한, HeMN의 파라미터 (target successful transmission probability, block size, 그리고 timeout)가 AoI에 미치는 영향을 분석하였고 trade-off 관계가 있음을 보였다. 마지막으로 HeMN에 저장되는 데이터를 신선하게 관리할 수 있도록 시스템 설계 방향을 제시하였다.

핵심어: 정보의 최신성, 블록체인, 하이퍼레저 패브릭, 지연 시간, stochastic geometry